Atomic physics of high-energy density and radiation-driven plasmas

Roberto C. Mancini

Physics Department, University of Nevada, Reno

High-Energy Density Science Center Seminar, LLNL, December 14th 2017

Students, post-docs, and collaborators

- I. Golovkin (Ph.D. 2000, Prism), P. Hakel (Ph.D. 2001, LANL), M. Sherrill (Ph.D. 2003, LANL), L. Welser-Sherrill (Ph.D. 2006, LANL), T. Nagayama (Ph.D. 2010, SNL), H. Johns (Ph.D. 2013, LANL), T. Joshi (Ph.D. 2015, LANL), T. Lockard (Ph.D. 2016, LLNL)
- R. Florido, ULPGC, Spain
- I. M. Hall, Diamond Light Source, UK
- R. Heeter, C. Iglesias, J. Kane, D. Liedahl, D. Martinez, H. Scott, V. Smalyuk, R. Tommasini, LLNL
- J. Delettrez, S. Regan, R. Shah, LLE, UR
- J. Bailey, G. Loisel, G. Rochau, SNL
- J. Abdallah, Jr., C. Fontes, S. Hsu, LANL
- T. Kallman, NASA

The impact of atomic physics

- Atomic processes and plasma atomic kinetics determine,
  - ion charge state distribution and level populations
  - photon energy dependent emissivity and opacity
  - emission, absorption and transport of radiation
  - also to some extent, EOS and thermal transport

- Plasma perturbations result in Stark broadened line shapes

- As a consequence, atomic physics plays a key role in **both** the diagnosis and modeling of plasmas

- We illustrate and discuss these ideas with two examples,
  - plasma diagnosis: tracer x-ray spectroscopy of inertial confinement fusion implosions
  - plasma modeling: heating of photoionized plasmas driven by a broadband x-ray flux

X-ray spectroscopy of ICF implosions

- X-ray spectroscopy has proven to be a powerful method to diagnose inertial confinement fusion experiments

- Analysis of the emission/absorption spectrum from a suitable tracer element added to the core and/or shell permits the diagnosis of the plasma conditions under which the emergent x-ray intensity distribution was formed

- The fundamental theory of plasma x-ray spectroscopy is multi-disciplinary: atomic, plasma and radiation transport physics

- The important and useful theory result is the dependence of the tracer's spectral features on plasma environmental conditions

- Important: test analysis method with synthetic data

Plasma environment drives excitations and perturbations

Argon Heβ (1-3) line spectrum: parent and satellite transitions

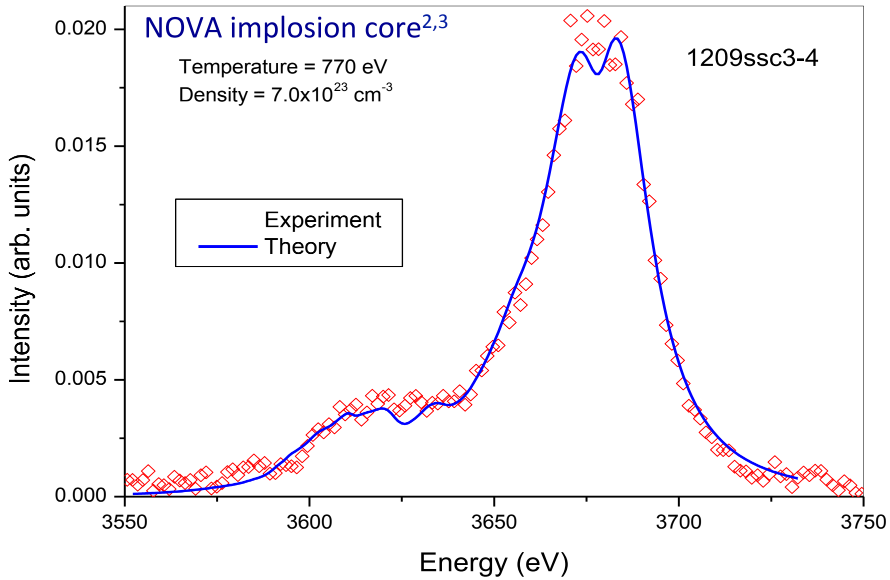

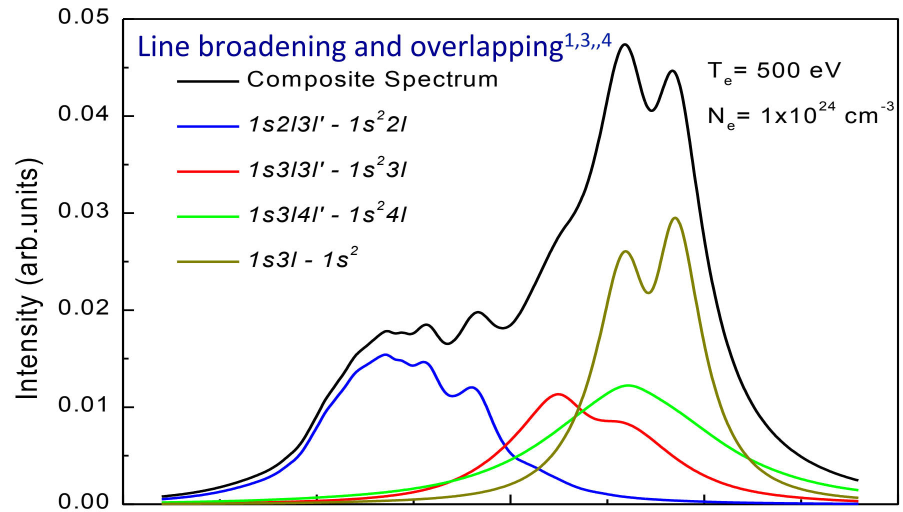

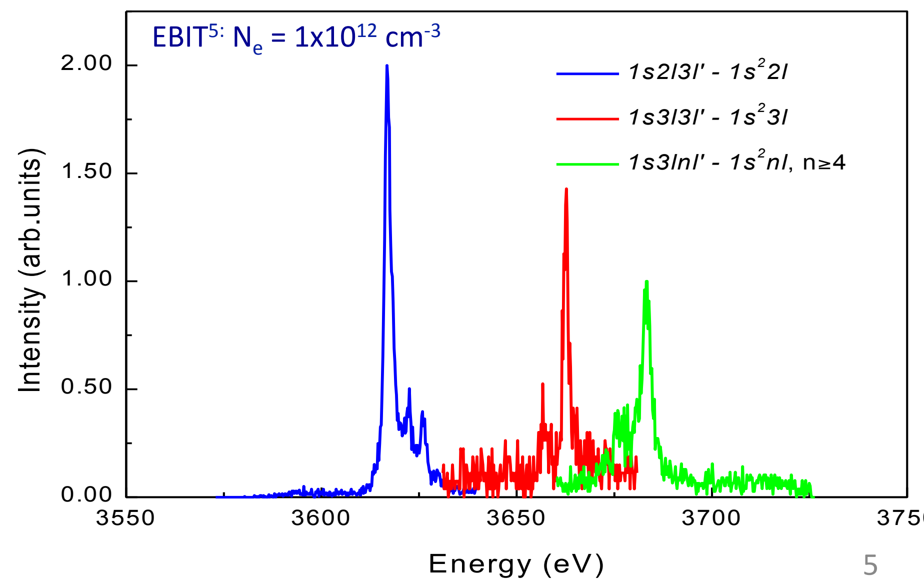

- 12 orders of magnitude in density change the physics and make a difference!
- Implosion core plasma is "rich" in atomic processes and perturbations

[1]R. C. Mancini, C. F. Hooper, Jr. et al, RSI **63**, 5119 (1992)
[2]N. C. Woolsey, B. A. Hammel et al, PRE **57**, 4650 (1998)
[3]I. E. Golovkin and R. C. Mancini, JQSRT **65**, 273 (2000)
[4]R. C. Mancini, C. A. Iglesias, S. Ferri et al HEDP **9**, 731 (2013)
[5]A. J. Smith, P. Beiersdorfer, V. Decaux et al, PRA **54**, 462 (1996)

Argon line ratios and widths

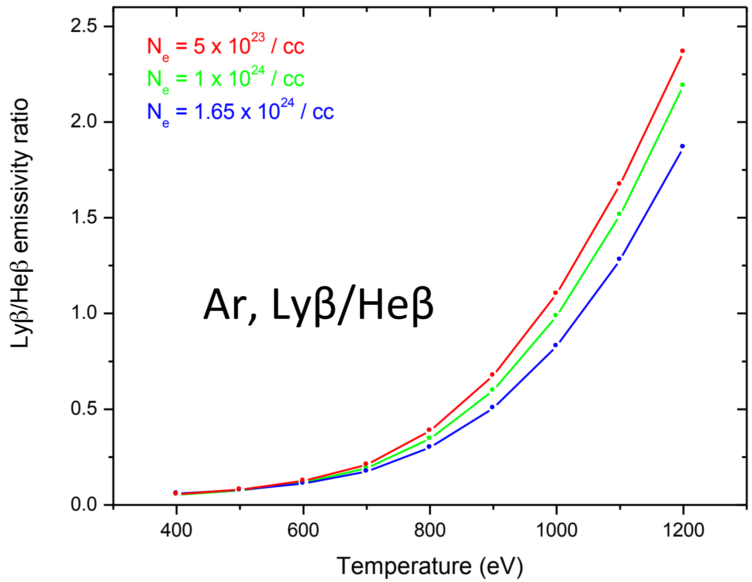

- Useful information is encoded in line ratios and widths that can be extracted from x-ray spectrometer observations
- But, in dense implosion core plasmas Stark line broadening, overlapping and blending make it difficult to isolate individual lines

He-like Ar Heβ

$1s^2\ ^1S_0 - 1s\ 3p\ ^1P_1$

$1s^2\ ^1S_0 - 1s\ 3p\ ^3P_1$

H-like Ar Lyβ

$1s\ ^2S_{1/2} - 3p\ ^2P_{1/2}$

$1s\ ^2S_{1/2} - 3p\ ^2P_{3/2}$

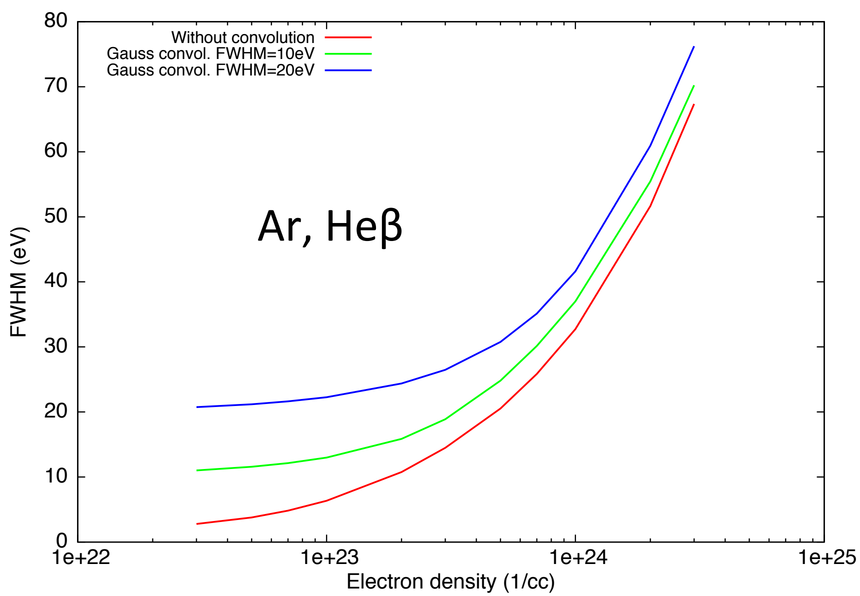

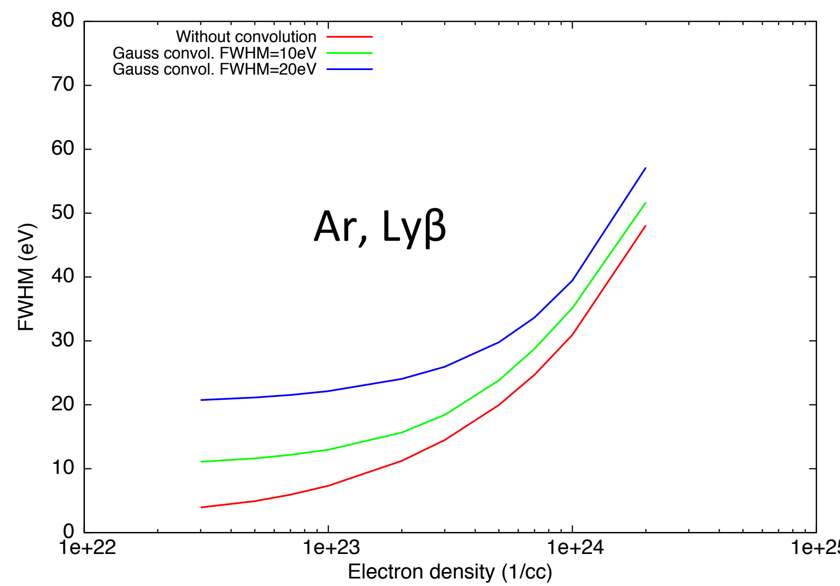

T_e and N_e dependence of argon K-shell spectra

Emergent intensity distribution is T_e and N_e dependent through the sensitivities of level population distribution and Stark-broadened spectral line shapes

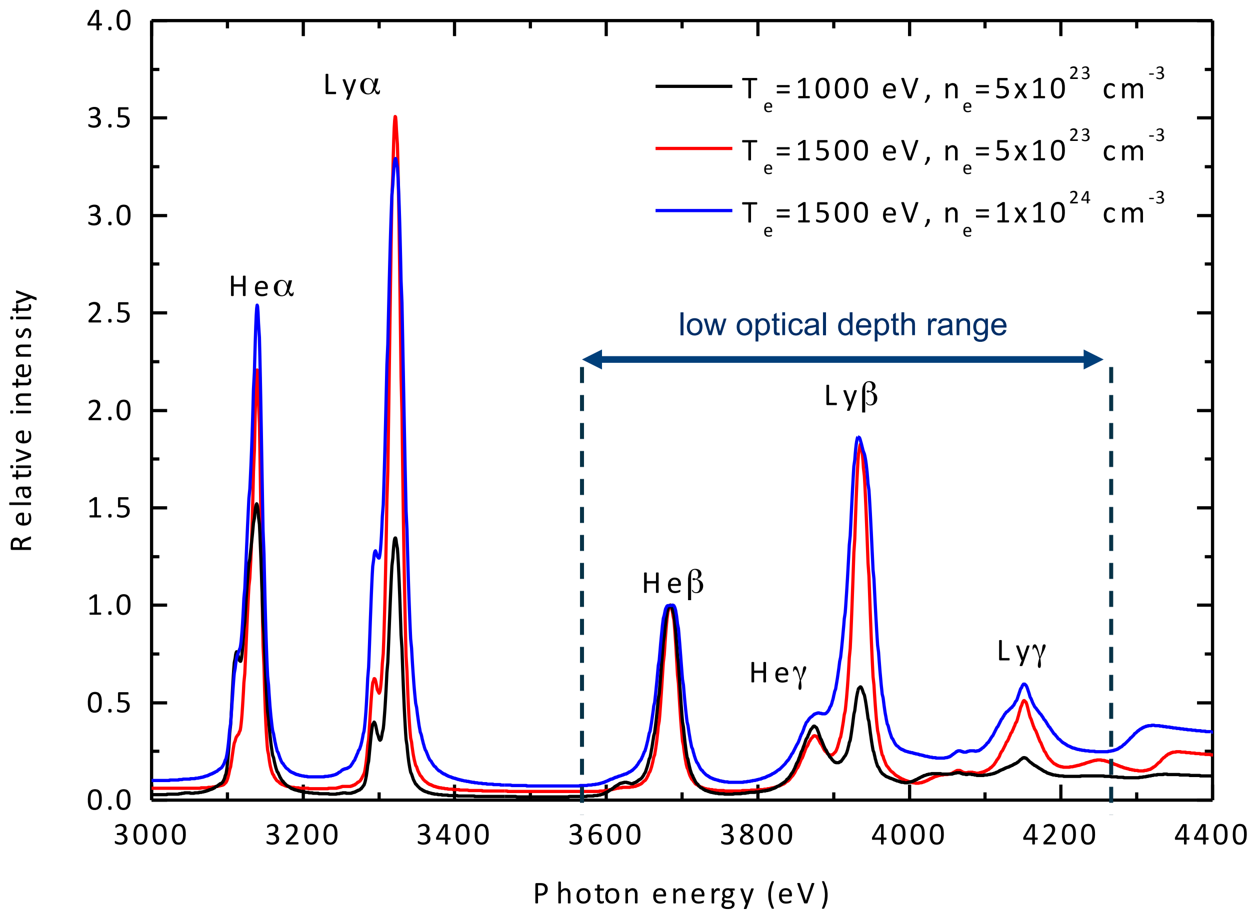

[1]R. Florido, R. C. Mancini, T. Nagayama, R. Tommasini, J. A. Delettrez, S. P. Regan, V. A. Smalyuk et al, High Energy Density Physics **6**, 70 (2010)

The atomic physics of x-ray spectroscopy

- Modeling and interpretation of x-ray spectroscopy of ICF experiments relies on atomic physics

- The emergent intensity distribution is T_e and N_e dependent through the T_e and N_e sensitivity of the atomic level population distribution and the N_e dependence of the Stark-broadened spectral line shapes

- There is also dependence on T_i through the ion dynamics contribution to Stark broadening, Doppler broadening, and the ion microfield distribution function

- The results of the x-ray spectroscopy enable other discussions and findings relevant to ICF physics

OMEGA direct-drive implosions

- Amount of Ar and Ti tracers has to be small:
  - Not to change the hydrodynamics
  - To keep the optical depth of the line transitions used for spectroscopic analysis small
  - Ti-doped: 2% atomic/1µm thick embedded or 3-6% atomic/0.5µm thick on inner shell surface
  - 5, 10 or 20 atmospheres of D_2 gas, doped with 0.072 atm of argon
  - Plastic shell thickness: 15, 20, 27, 40 microns

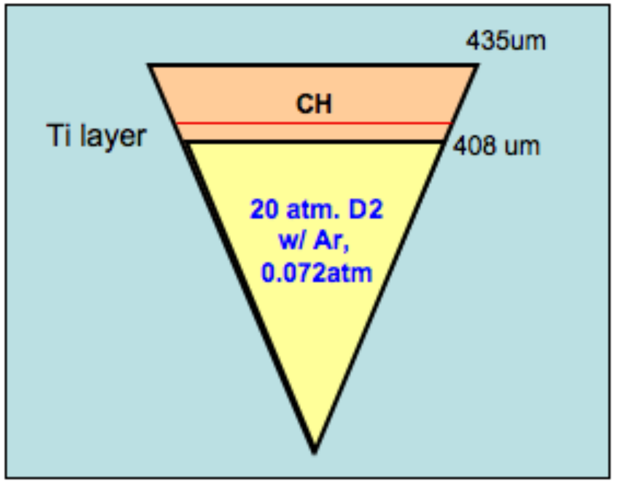

- Laser:
  - 1ns-sq, α2, α3 & shock-ignition pulse shapes
  - 60 beams, 20kJ to 23kJ UVOT
  - Smoothing: 2D-SSD/DPP-SG4/DPR

- Three x-ray spectrometers:
  - XRS1: crystal spectrometer (ADP)
  - SSCA: streaked, crystal spectrometer (RbAP)
  - MMI: multi-monochromatic x-ray imager (MLM)

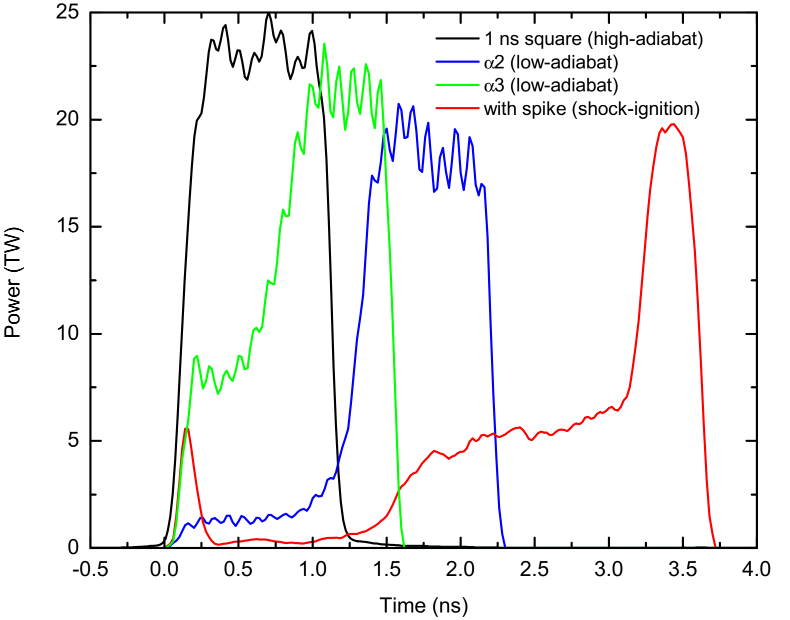

Streaked spectrometer provides time histories

Streaked argon spectrum and compression continuum[1,2]

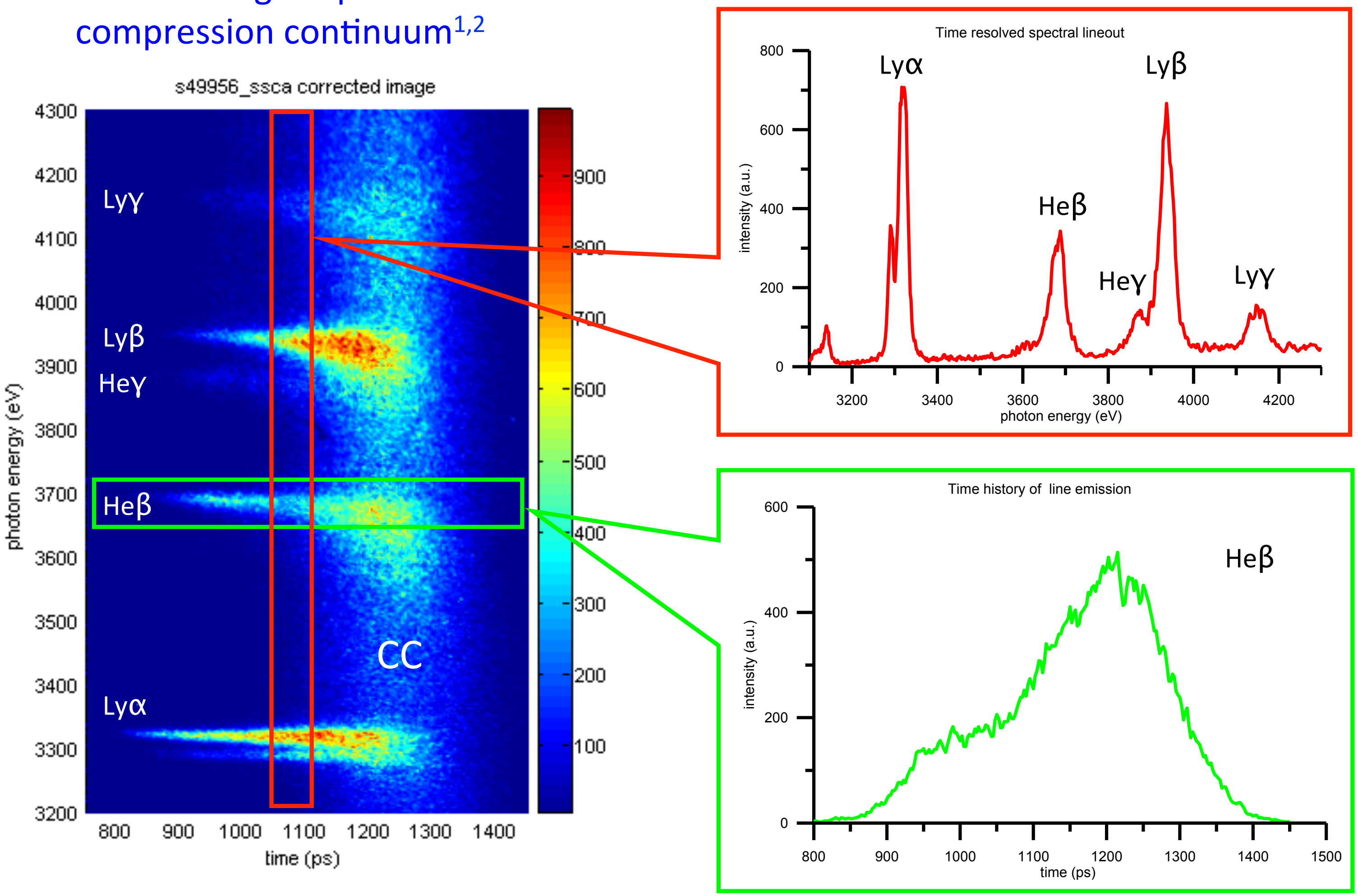

Time-resolved spectrum

Time history of narrow-band

[1]S. P. Regan, J. A. Delettrez, R. Epstein, P. A. Jaanimagi, B. Yaakobi, V. A. Smalyuk, F. J. Marshall et al, Phys. Plasmas **9**, 1357 (2002)
[2]R. Florido, T. Nagayama, R. C. Mancini, R. Tommasini, J. Delettrez, S. P. Regan et al, Rev. Scientific Instruments **79**, 10E310 (2008)

Diagnostic time-correlation based on physics events

Argon K-shell x-ray spectroscopy diagnoses core plasma burning conditions

SSC1: x-ray crystal streaked spectrometer, **NTD**: neutron temporal diagnostic

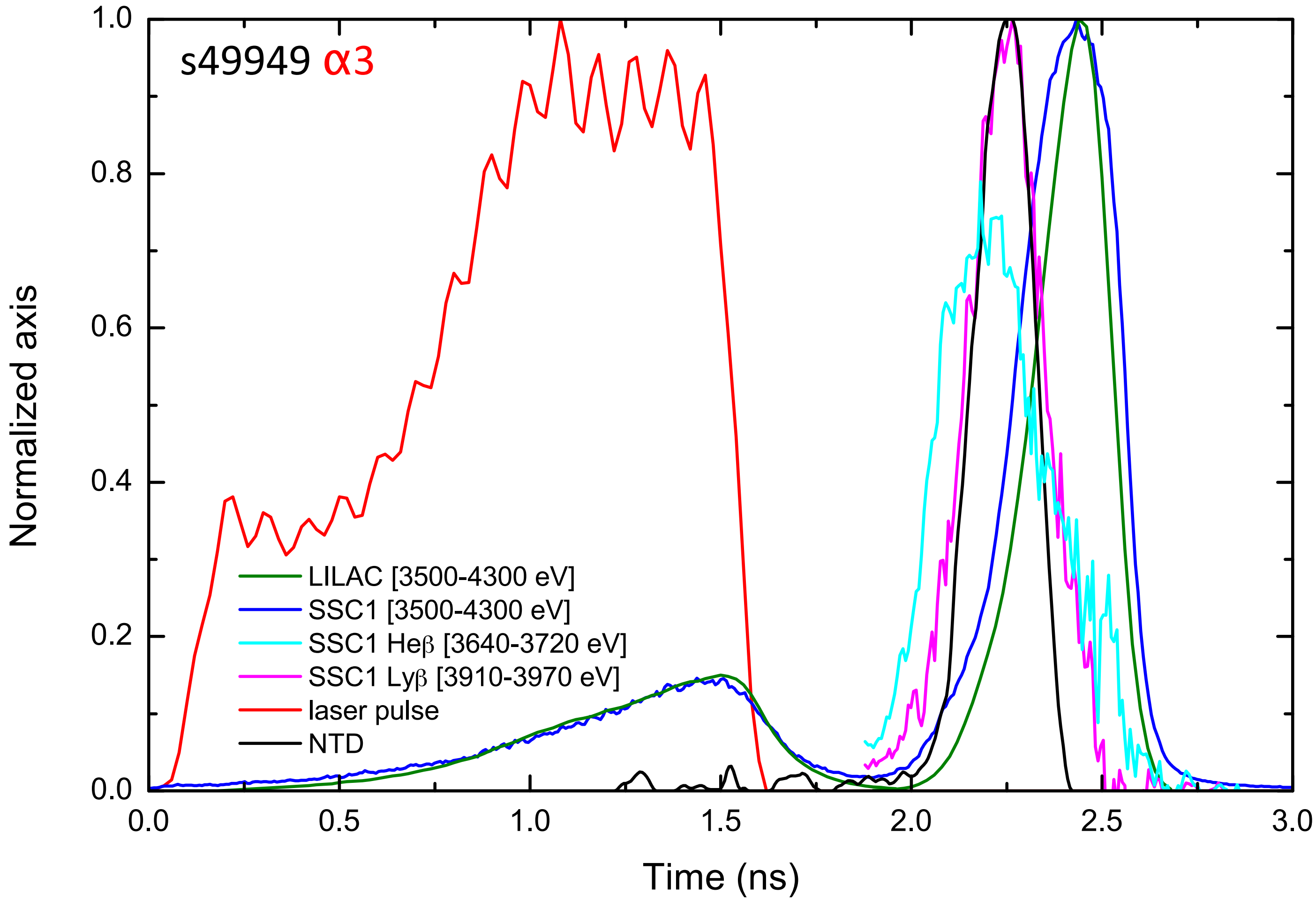

Theory produces good approximations to data

Spectroscopic analysis is based on argon β (1-3) and γ (1-4) lines[1]

T_e=1300 ± 70 eV, n_e=5.0 ± 0.5 ×10^{23} cm^{-3} T_e=1450 ± 80 eV, n_e=1.4 ± 0.2 ×10^{24} cm^{-3} T_e=1270 ± 70 eV, n_e=3.1 ± 0.6 ×10^{24} cm^{-3}

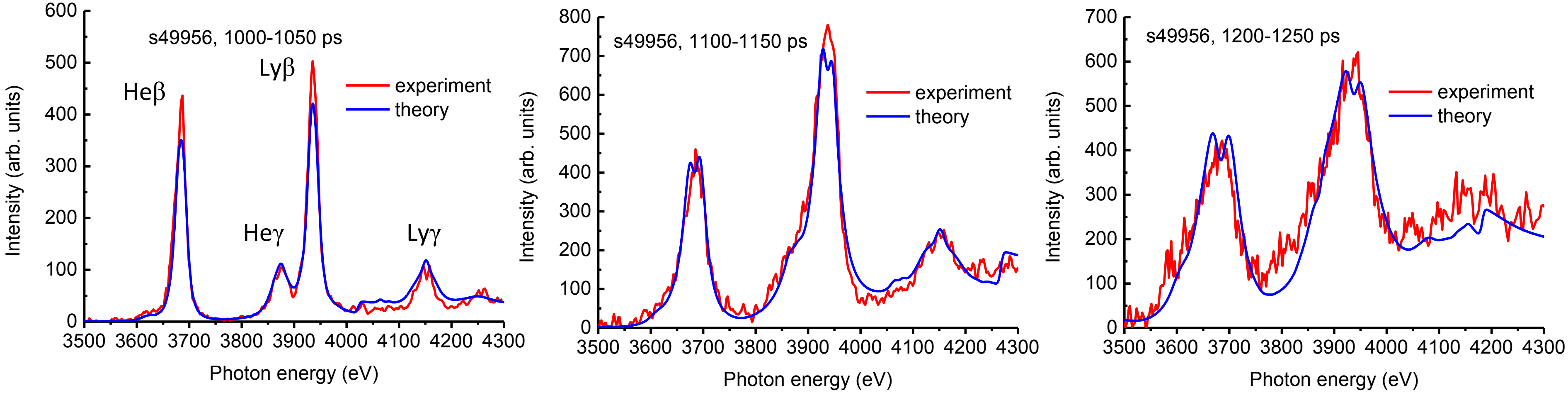

- Instrumental broadening included, FWHM=9eV
- Each spectrum is representative of Δt=50ps
- Steady state approximation[2] good for $N_e > 1\times10^{22}$ cm^{-3}
- ρ [g/cm^3] ≈ 3.24×N_e [10^{24} cm^{-3}]
- Changes in tracer spectra reflect T_e and N_e conditions in core plasma

[1]R. Florido, R. C. Mancini, T. Nagayama, R. Tommasini, J. A. Delettrez, S. P. Regan, V. A. Smalyuk et al, High Energy Density Physics **6**, 70 (2010)
[2]R. Florido and R. C. Mancini, Journal of Physics B **48**, 224006 (2015)

T_e and N_e time–histories of α2 implosions

Low- (α2) and high-adiabat (1ns-square) pulses drive different core hydrodynamics

1ns-square

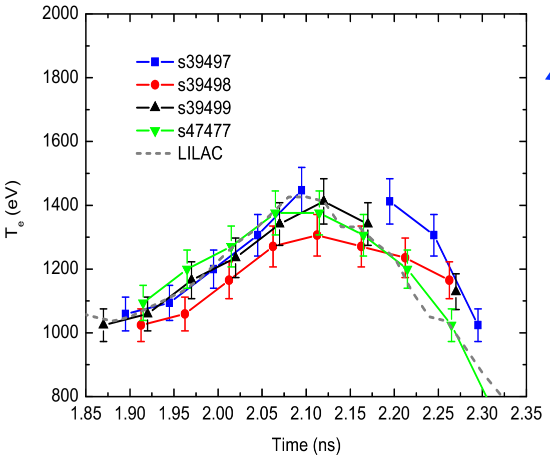

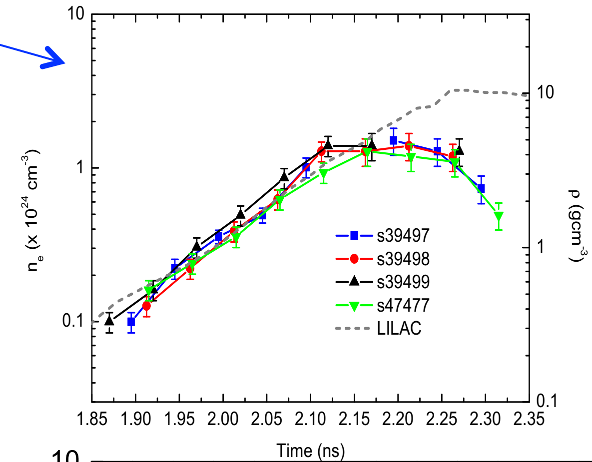

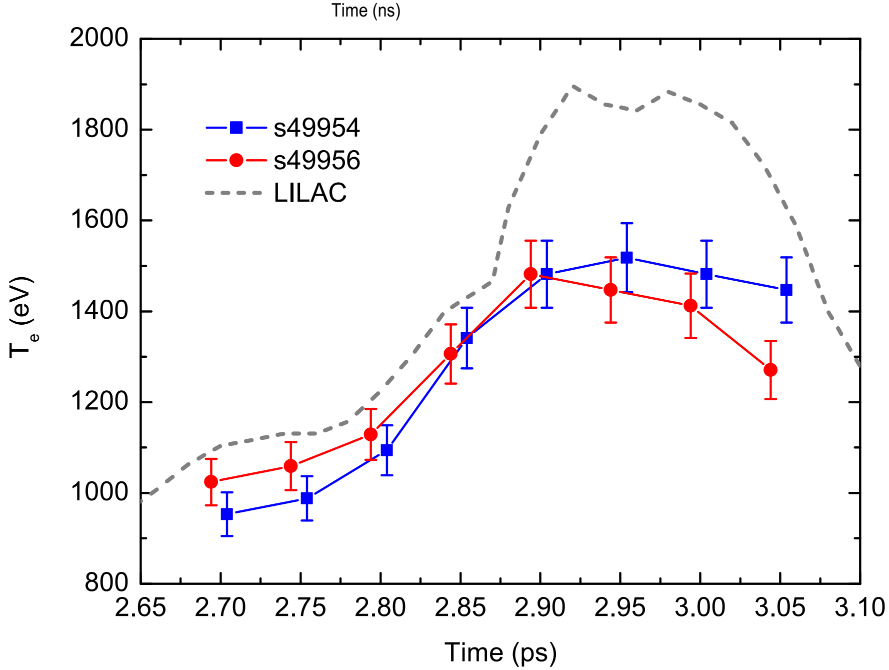

α2

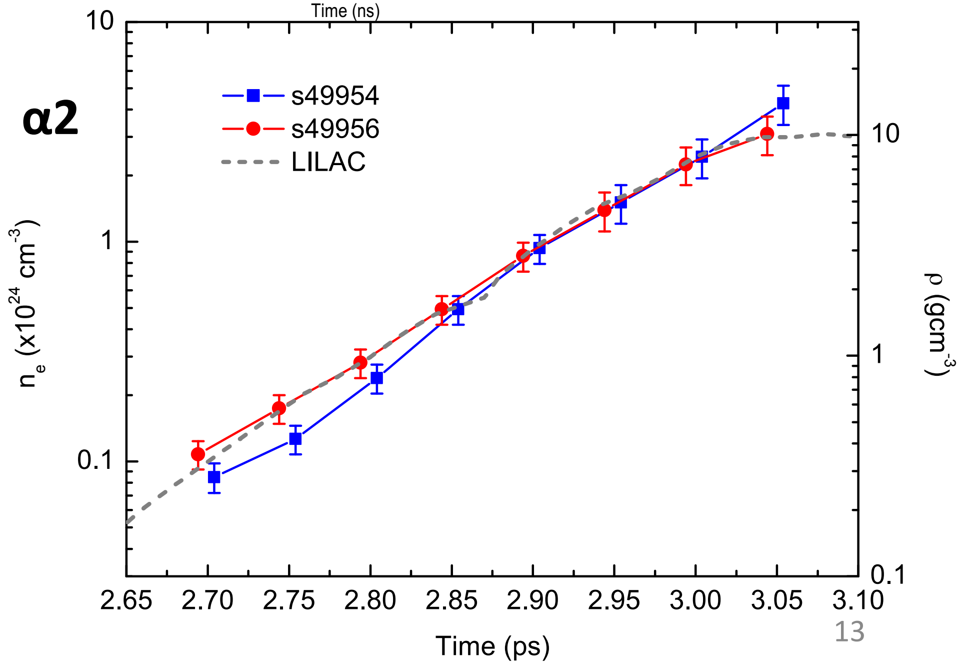

T_e and N_e time-histories of α3 implosions

Low-adiabat α3 produce more heating than α2 and comparable compression

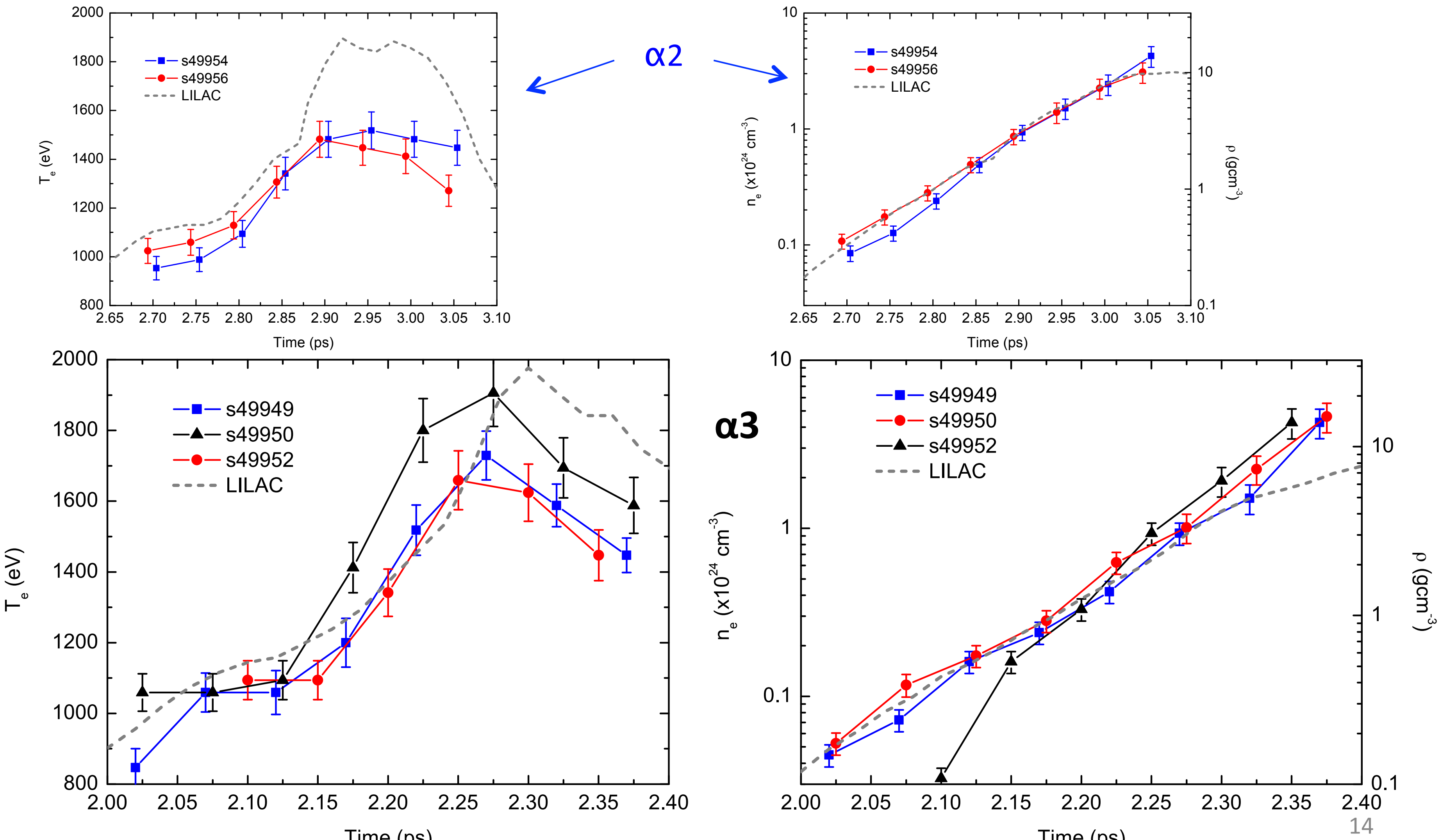

Time-history of SI dense shell optical depth

Experiment optical depth disagrees with simulation result[1]

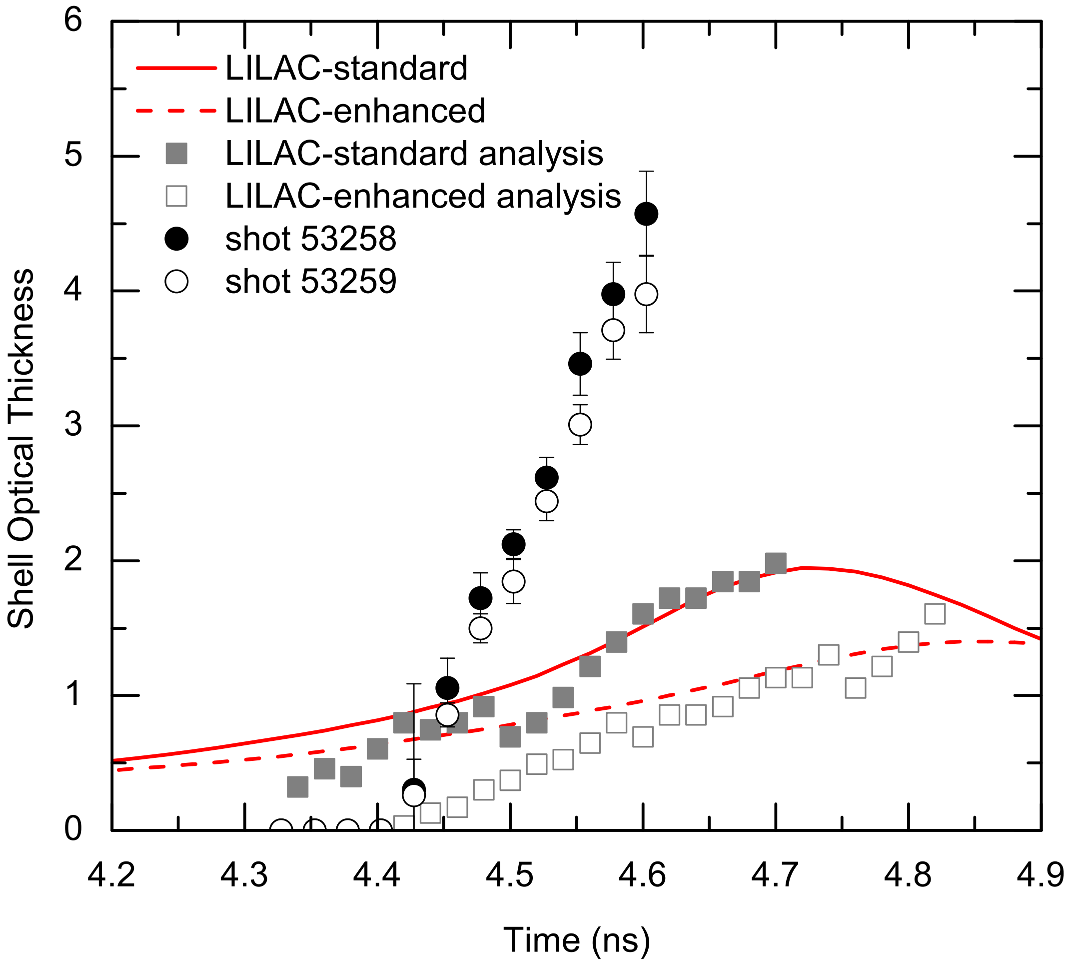

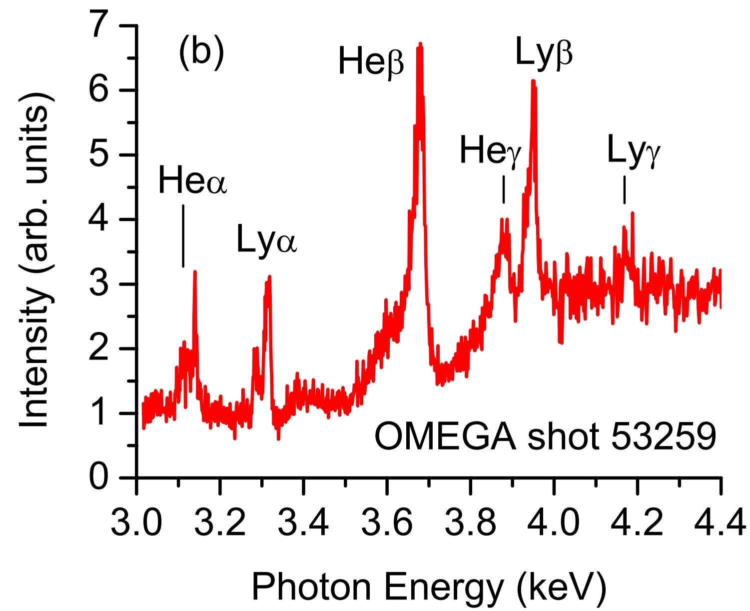

- Photon energy dependent attenuation produces a spectral modulation useful for dense shell diagnosis[2]

[1] R. Florido, R. C. Mancini, T. Nagayama, R. Tommasini, J. A. Delettrez, S. P. Regan and B. Yaakobi Phys. Review E **83**, 066408 (2011)
[2] B. Yaakobi, R. Epstein and F. J. Marshall, Phys. Rev. A **44**, 8429 (1991)

T_e and N_e time-histories of SI implosion core

- Shock ignition (SI) implosion cores have also been diagnosed with x-rayspectroscopy[1]
- Thick shell (40μm) produces a characteristic attenuation of the core's argon emission
- **Experiment and simulation show different core heating dynamics**

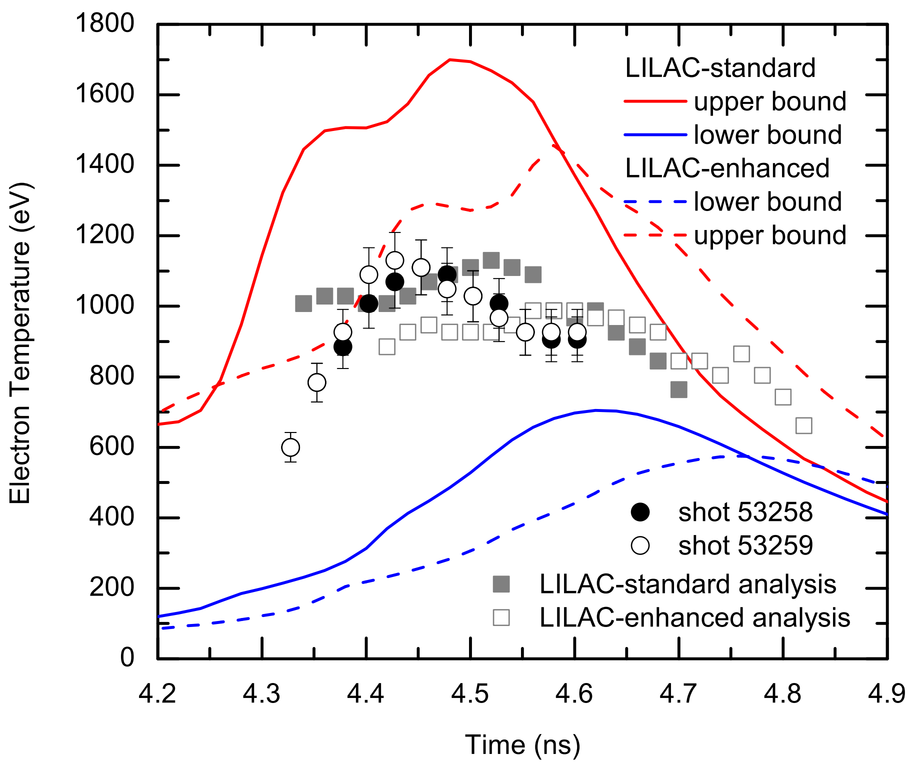

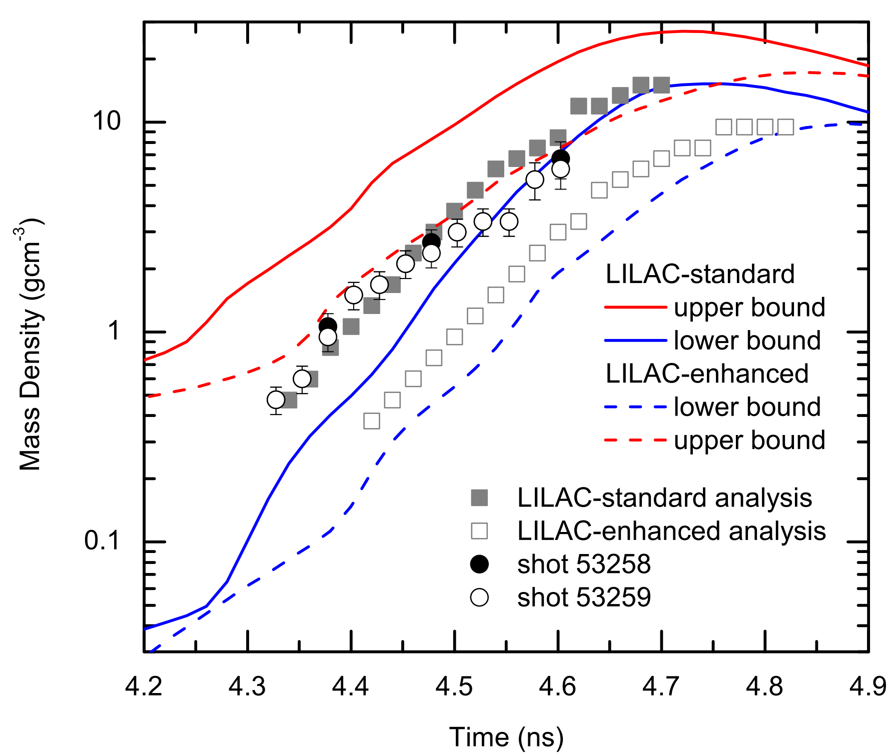

[1]R. Florido, R. C. Mancini, T. Nagayama, R. Tommasini, J. A. Delettrez and S. P. Regan, Physics of Plasmas **21**, 102709 (2014)

Core compression: a polytropic process

The results of the spectroscopic analysis suggest an interpretation of the implosion deceleration and core compression as a two-stage polytropic process of index γ

Shot	Type	Temperature	γ
49949	α3	increasing	1.23 ± 0.03
		decreasing	0.89 ± 0.07
49950	α3	increasing	1.13 ± 0.03
		decreasing	0.91 ± 0.07
49952	α3	increasing	1.24 ± 0.03
		decreasing	0.88 ± 0.07
49954	α2	increasing	1.17 ± 0.03
		decreasing	0.95 ± 0.10
49956	α2	increasing	1.19 ± 0.05
		decreasing	0.89 ± 0.08
53528	SI	increasing	1.39 ±0.07
		decreasing	0.80 ±0.08
53529	SI	increasing	1.47 ±0.08
		decreasing	0.82 ±0.07

Polytropic process:

$$T = C\rho^{\gamma-1}$$

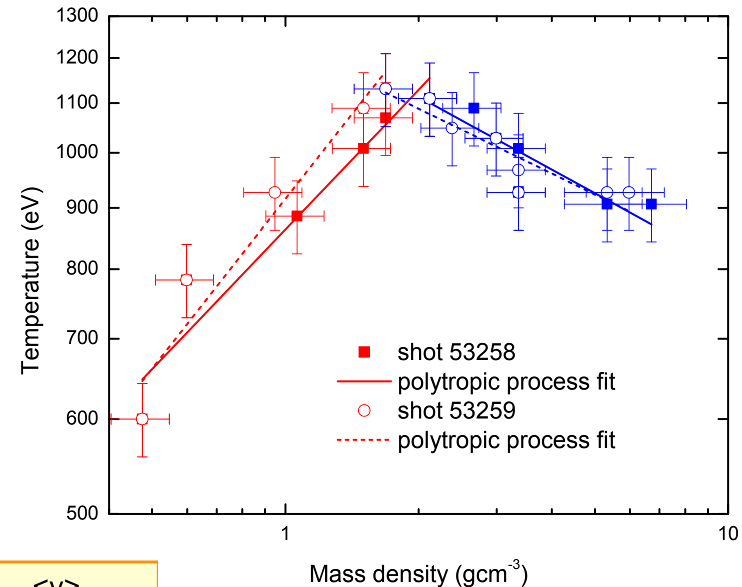

Type	Temperature	<γ>
α3	increasing	1.20 ± 0.03
	decreasing	0.89 ± 0.07
α2	increasing	1.18 ± 0.04
	decreasing	0.92 ± 0.09
SI	increasing	1.43 ±0.08
	decreasing	0.81±0.08

SI LILAC results

SI	LILAC std	LILAC enh
increasing	1.05	1.05
decreasing	0.72	0.82

- **Differences in γ indicate differences in energy exchange between core and shell**

Implosion core energy balance analysis

X-ray spectroscopy results enable energy balance analysis of the core[1]

Energy conservation: $$\frac{dE}{dt} = \frac{d}{dt}(U + K) = \dot{W} + \dot{F} + \dot{J}$$

U: internal energy, ***K***: kinetic energy, ***W***: volume work, ***F***: heat flux, ***J***: radiation flux

Energy terms (*J*)		LILAC simulation		Synthetic spectra analysis		Experiment	
		Standard	Enhanced	Standard	Enhanced	Shot 53258	Shot 53259
	ΔW	77.05	46.11	83.86	50.06	73.50	68.37
1st stage	ΔF	−4.35	−2.32	−10.97	−7.93	−9.01	−7.61
Increasing *T*	ΔJ	−28.21	−18.09	−16.11	−8.21	−8.16	−5.64
	ΔE	44.49	25.70	56.78	33.92	56.33	55.12
	ΔW	84.38	55.13	84.75	63.41	92.89	104.92
2nd stage	ΔF	−10.88	−5.74	−9.48	−7.50	−11.26	−13.95
Decreasing *T*	ΔJ	−89.65	−49.94	−73.66	−46.53	−32.57	−34.56
	ΔE	−16.15	−0.55	1.61	9.38	49.06	56.41
	ΔW	161.43	101.24	168.61	113.47	166.39	173.29
Entire	ΔF	−15.23	−8.06	−20.45	−15.43	−20.27	−21.56
Time interval	ΔJ	−117.86	−68.03	−89.77	−54.74	−40.73	−40.20
	ΔE	28.34	25.15	58.39	43.30	105.39	111.53

[1]R. Florido, R. C. Mancini, T. Nagayama, R. Tommasini, J. A. Delettrez and S. P. Regan, Physics of Plasmas **21**, 102709 (2014)

Spectrally resolved imaging with MMI

MMI ≡ multi-monochromatic x-ray imager

- The OMEGA MMI was jointly developed by a UNR-LLNL collaboration as part of NLUF projects[1-4]
- A pinhole-array coupled to a multi-layer Bragg mirror records arrays of gated, spectrally resolved images on a MCP based detector

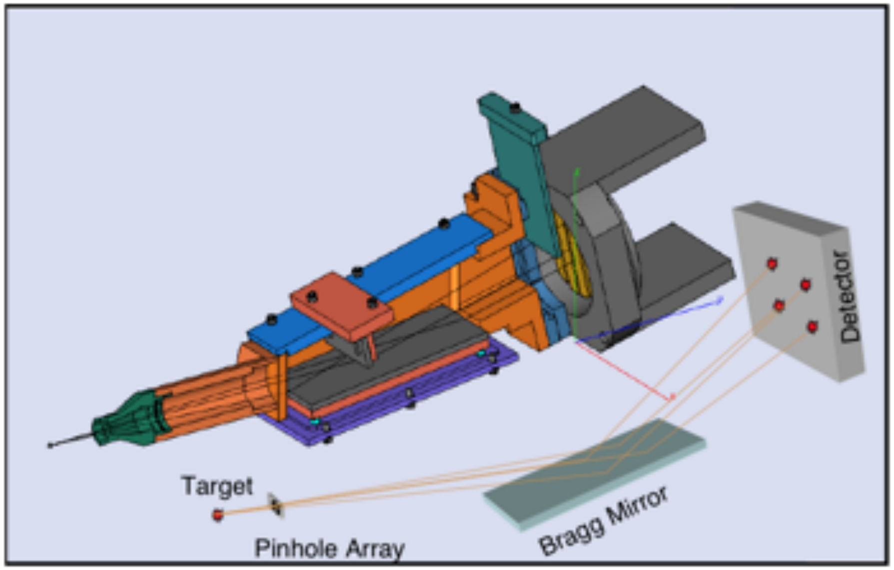

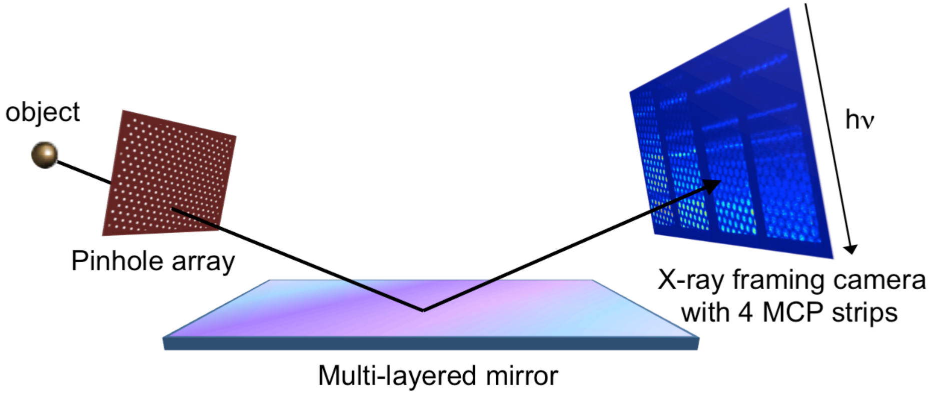

[1]L. Welser, R. C. Mancini, J. A. Koch, S. Dalhed, R. W. Lee, I. E. Golovkin et al, Rev. Sci. Instrum. **74**, 1951 (2003)
[2]J. A. Koch, T. W. Barbee, Jr., N. Izumi, R. Tommasini, R. C. Mancini et al, Rev. Sci. Instrum. **76**, 073708 (2005)
[3]R. Tommasini, J. Koch, N. Izumi, L. Welser, R. C. Mancini, J. Delettrez et al, Rev. Sci. Instrum. **77**, 10E303 (2006)
[4]T. Nagayama, R. C. Mancini, R. Florido, R. Tommasini, J. Koch et al, J. Applied Physics **109**, 093303 (2011)

MMI records arrays of spectrally resolved images

- Resolution: $\Delta x \approx 10\ \mu m$, $E/\Delta E \approx 150$
- M = 8.1
- Frame separation: 100 ps

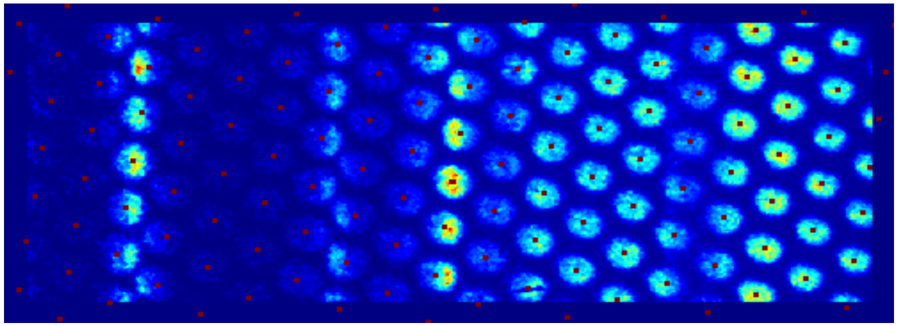

- Provided spatial sampling width is **smaller** than spectral width, MMI can be processed to obtain[1,2]:

Narrow-band (Heβ)

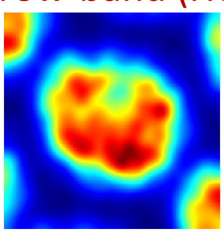

Broad-band

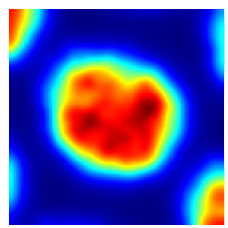

Space-integrated spectrum

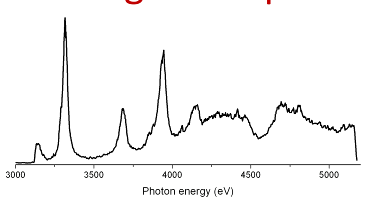

Space-resolved spectrum

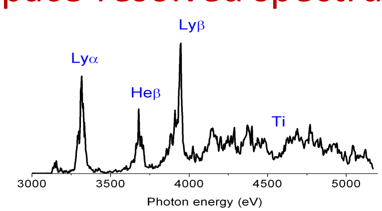

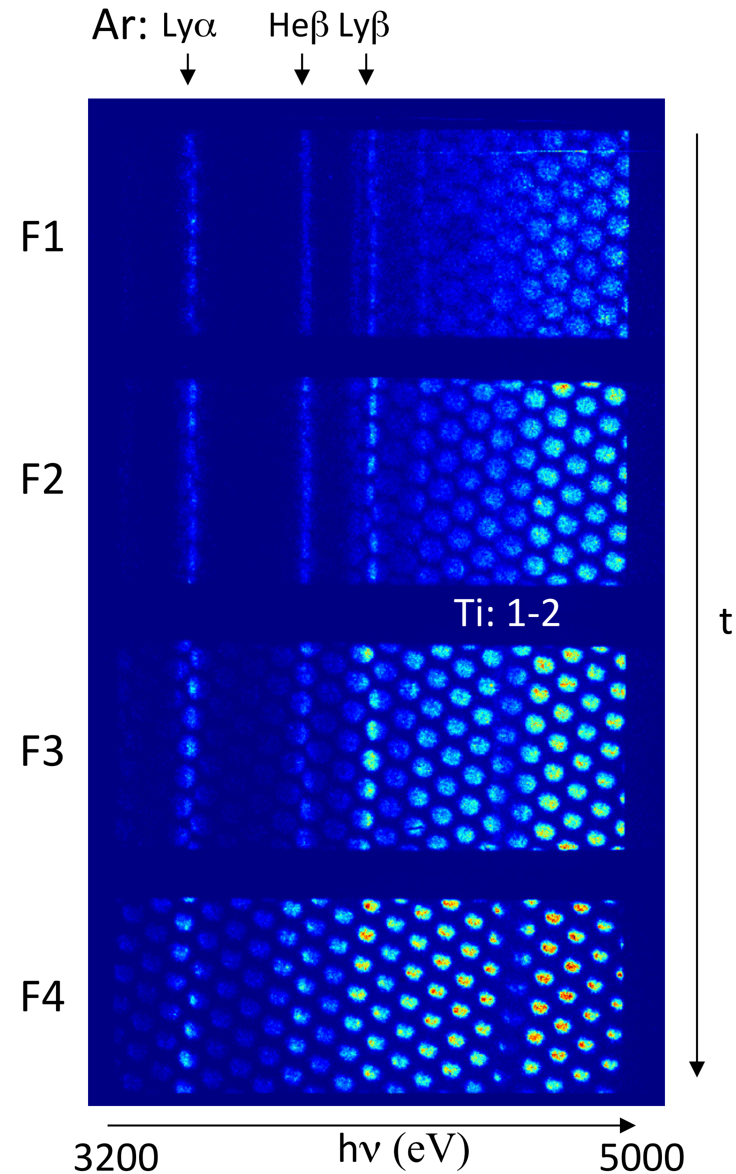

[1]T. Nagayama, R. C. Mancini, R. Mayes, R. Tommasini, R. Florido, High Power Laser Science and Engineering **3**, e23 (2015)

[2]R. C. Mancini, H. M. Johns, T. Joshi, D. Mayes, T. Nagayama, S. C. Hsu, J. Baumgaertel, J. Cobble et al, Phys. Plasmas **21**, 122704 (2014)

Spatially resolved spectra from spectrally resolved images

Contributions are taken **only** from a selected region of the image as a function of photon energy

Rectangular regions

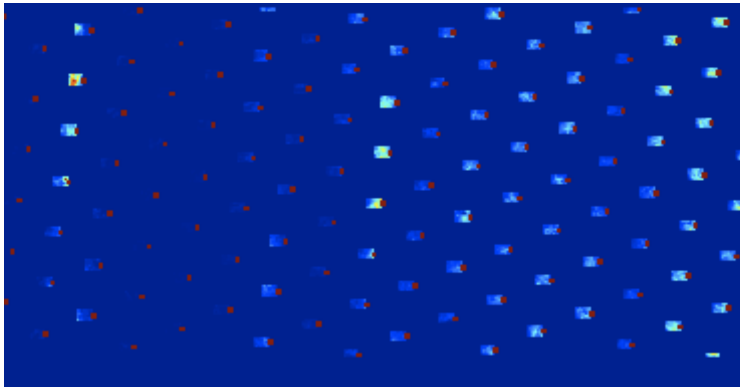

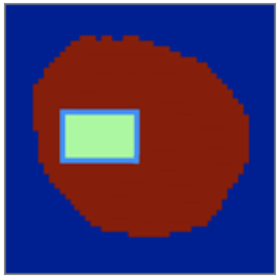

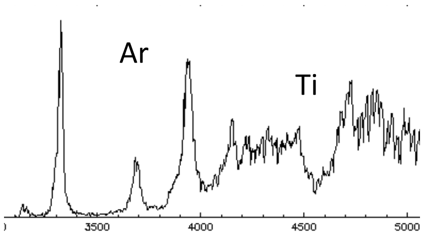

Useful for 3D polychromatic tomography[1], and extraction of areal-density maps[2,3]

Annular regions

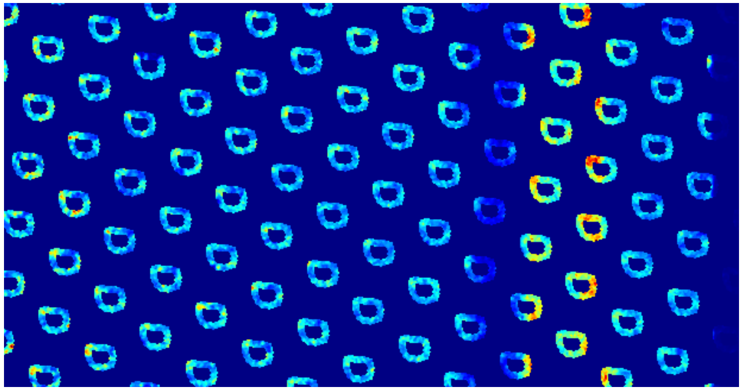

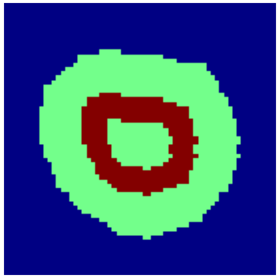

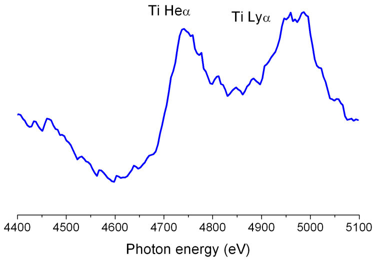

Useful for tracking tracer distribution and migration into the core[4]

[1]T. Nagayama, R. C. Mancini, R.Florido, D. Mayes, R. Tommasini, J. A. Koch et al , Phys. Plasmas **19**, 082705 (2012)
[2]H. M. Johns, R. C. Mancini, P. Hakel, T. Nagayama, V. Smalyuk, S. P. Regan et al, Phys. Plasmas **21**, 082711 (2014)
[3]H. M. Johns, R. C. Mancini, T. Nagayama, D. C. Mayes, R. Tommasini, V. A. Smalyuk et al, Phys. Plasmas **23**, 012709 (2016)
[4]T. R. Joshi et al, in preparation for publication

Interpretation of spatially resolved spectra

- **The selection of image region defines the domain of integration in the core**[1]
- There is flexibility in the selection of the image region
- Limitations: spatial resolution, enough light

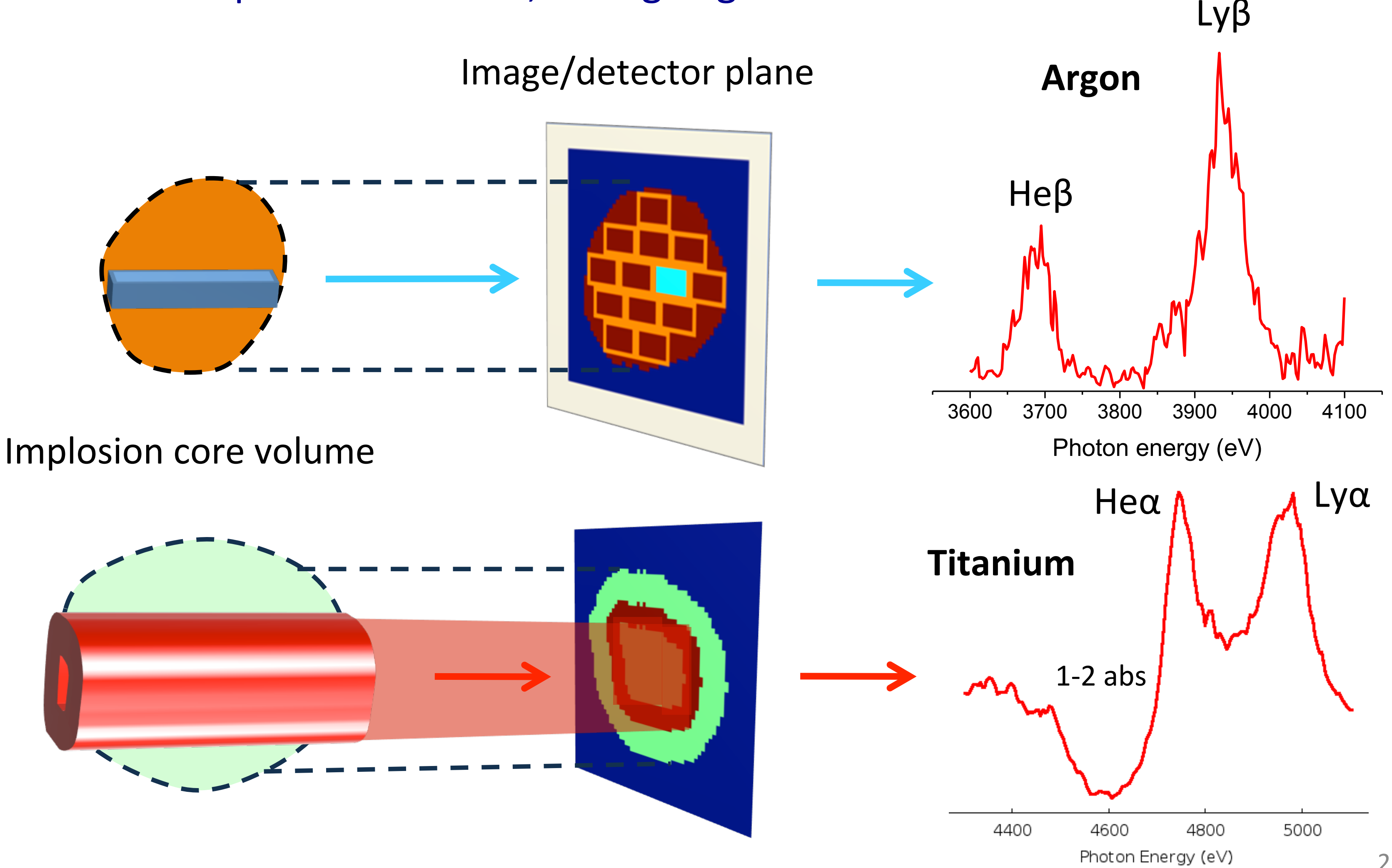

[1]T. Nagayama, R. C. Mancini, R. Florido, D. Mayes, R. Tommasini, J. Koch et al, Phys. Plasmas **21**, 050702 (2014)

Spatially resolved spectra from one LOS: TIM4

OMEGA shot 49956
TIM4, Frame3

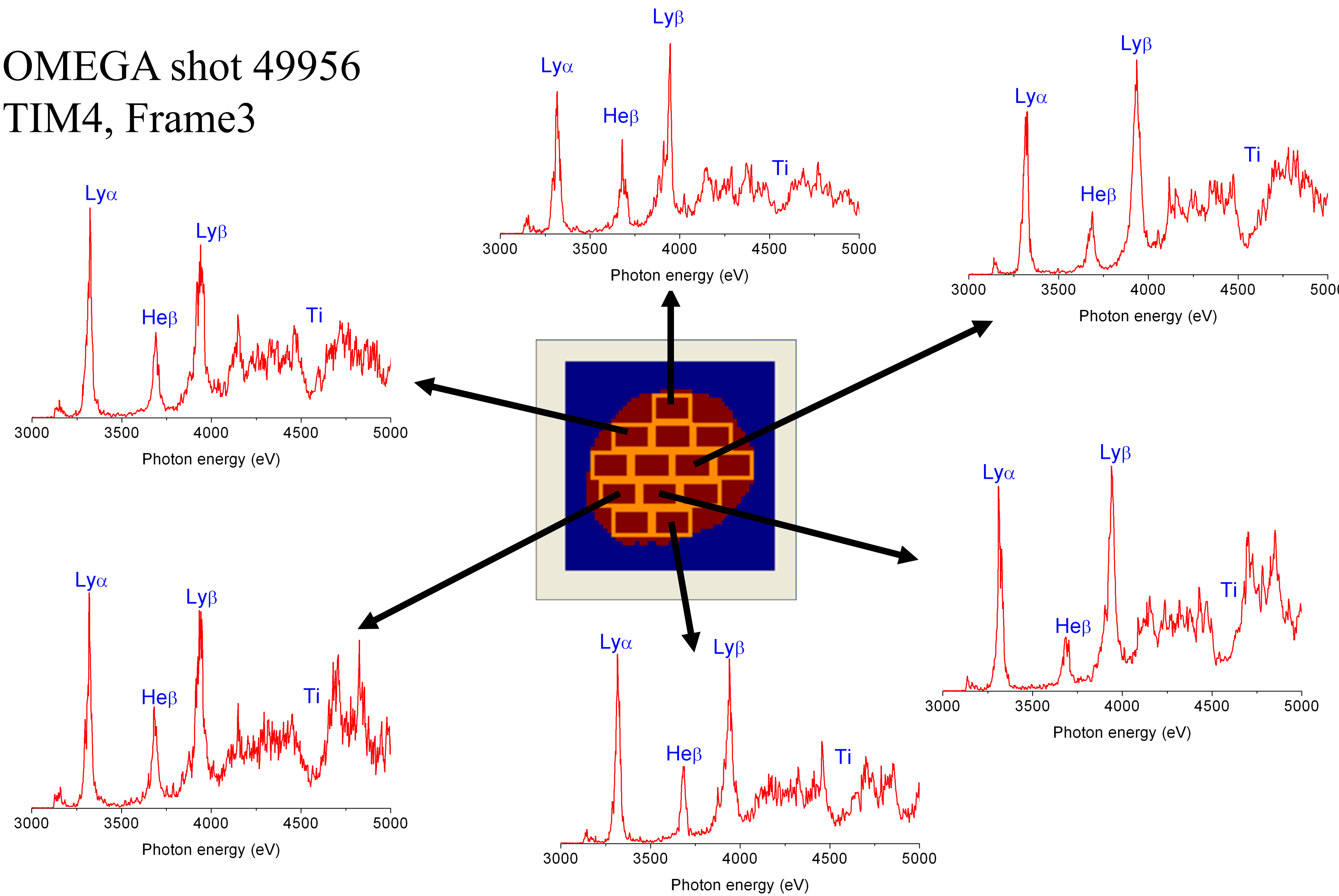

- **NOTE: independent analysis of each individual spectrum does not produce the spatial distribution of local T_e and N_e values inside the core**

The idea of multi-objective data analysis

- **Motivation:** what information can be extracted by **simultaneously and self-consistently** analyzing multiple pieces of data that cannot be extracted by considering **only** each single piece of data on an individual basis?
- **Idea:** search parameter space for model input that produces the best approximation to multiple pieces of data (objectives)
- In plasma spectroscopy, the need for this analysis arose in connection with the unfolding of the temperature and density distribution in an implosion core[1,2]
- A single measurement cannot provide a spatial distribution of local values
- The idea is general and can be applied to any type/combination of data

[1] I. Golovkin, R. Mancini, S. Louis, Y. Ochi, K. Fujita, H. Nishimura et al, Physical Review Letters **88**, 045002 (2002)
[2] R. Mancini, Ch. 15 in "*Applications of Multi-Objective Evolutionary Algorithms*" , Eds. C. Coello-Coello and G. Lamont, World Scientific Pub. ISBN 981-256-106-4 (2004)

Implementation of multi-objective analysis

- Need an optimization algorithm to conduct a smart search in parameter space, an exhaustive search is likely to be impractical
- Several options, we have primarily worked with genetic algorithms
- Genetic algorithms have successfully applied the mechanics of natural selection to a wide array of artificial problems[1,2]
- Pareto domination is a concept in multi-objective optimization that **tracks individual objectives** through the development of a Pareto front in fitness space
- A Pareto genetic algorithm (PGA) combines both concepts by including Pareto domination in the selection of members for the next generation[3]

[1] J. Holland, "Adaptation in natural and artificial systems" Pub. The University of Michigan Press, Ann Arbor (1975)
[2] D. Goldberg, "Genetic algorithms in search, optimization and machine learning" Pub. Addison-Wesley, Reading (1989)
[3] K. Deb, "Multi-Objective Optimization using Evolutionary Algorithms" Pub. John Wiley & Sons, New York (2001)

Multi-objective analysis with a PGA

- Multi-objective data analysis driven by a PGA can be applied to any type/combination of data
- The details of the Pareto front provide information about the properties of the problem, e.g. consistency of objectives or subsets of objectives
- With spectroscopic data, this method has been applied to extract the spatial-structure of implosion cores using different types and number of objectives:

1 image and 1 spectrum: 1D T_e and N_e spatial profiles in GEKKO DD implosion cores,
E. Golovkin, R. C. Mancini, S. Louis, Y. Ochi et al, Physical Review Letters **88**, 045002 (2002)
2 images and 1 spectrum: 1D T_e and N_e spatial profiles in OMEGA ID implosion cores,
L. A. Welser, R. C. Mancini, J. Koch et al, J. Quant. Spec. Radiative Transfer **99**, 649 (2006)
3 images (op. thin and thick) and 1 spectrum: quasi-2D T_e, N_e profiles in OMEGA ID cores,
L. A. Welser-Sherrill, R. C. Mancini, J. Koch, N. Izumi et al, Physical Review E **76**, 056403 (2007)
Arrays of spatially resolved spectra: 3D reconstruction of OMEGA DD implosion cores,
T. Nagayama, R. C. Mancini, R. Florido, R. Tommasini et al, Phys. Plasmas **19**, 082705 (2012)

Observations along three LOS provide the basis for a 3D reconstruction via polychromatic tomography[1]

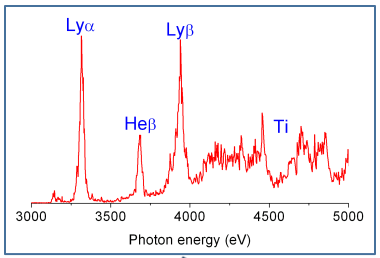

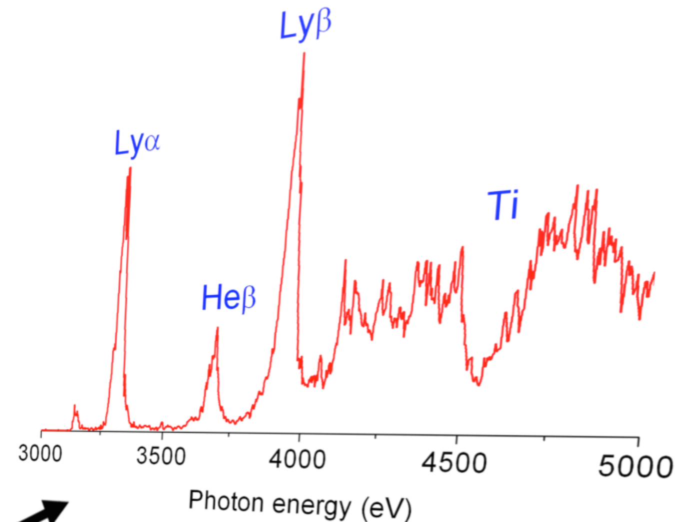

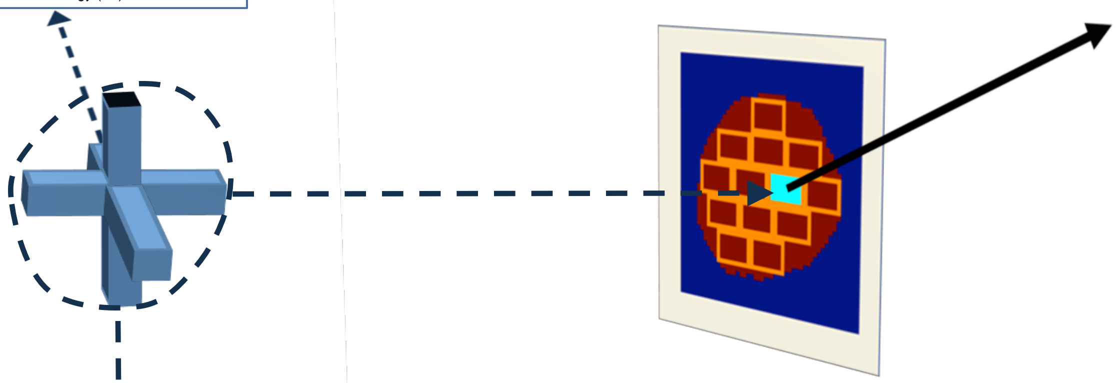

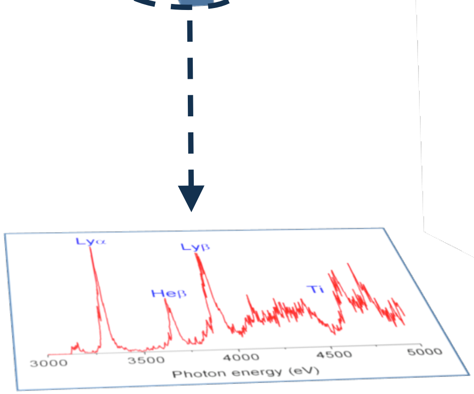

- Each space-resolved spectrum has temperature and density information integrated along chords parallel to each LOS and perpendicular to the image plane
- Each spatial region is located at a **unique** intersection of three chords
- Spatial regions are constrained by their contributions to spatially-resolved spectra recorded along three LOS

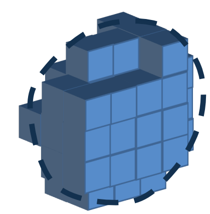

[1]T. Nagayama, R. C. Mancini, R.Florido, D. Mayes, R. Tommasini, J. Koch, J. Delettrez, S. P. Regan, V. Smalyuk, Phys. Plasmas **19**, 082705 (2012)

Extracted 3D T_e and N_e spatial distribution

- Polychromatic tomography extensively tested with synthetic data[1]
- OMEGA shot 49956, α2, 3 MMI's mounted on TIM3/4/5, Δt=100ps
- 141 spectra were used to extract T_e and N_e spatial structure
- Te tends to be larger in central region, Ne in the periphery
- 3D asymmetries in the spatial structures are observed

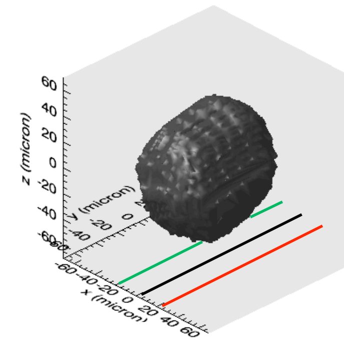

x = -21 μm   x = 0 μm   x = 21 μm

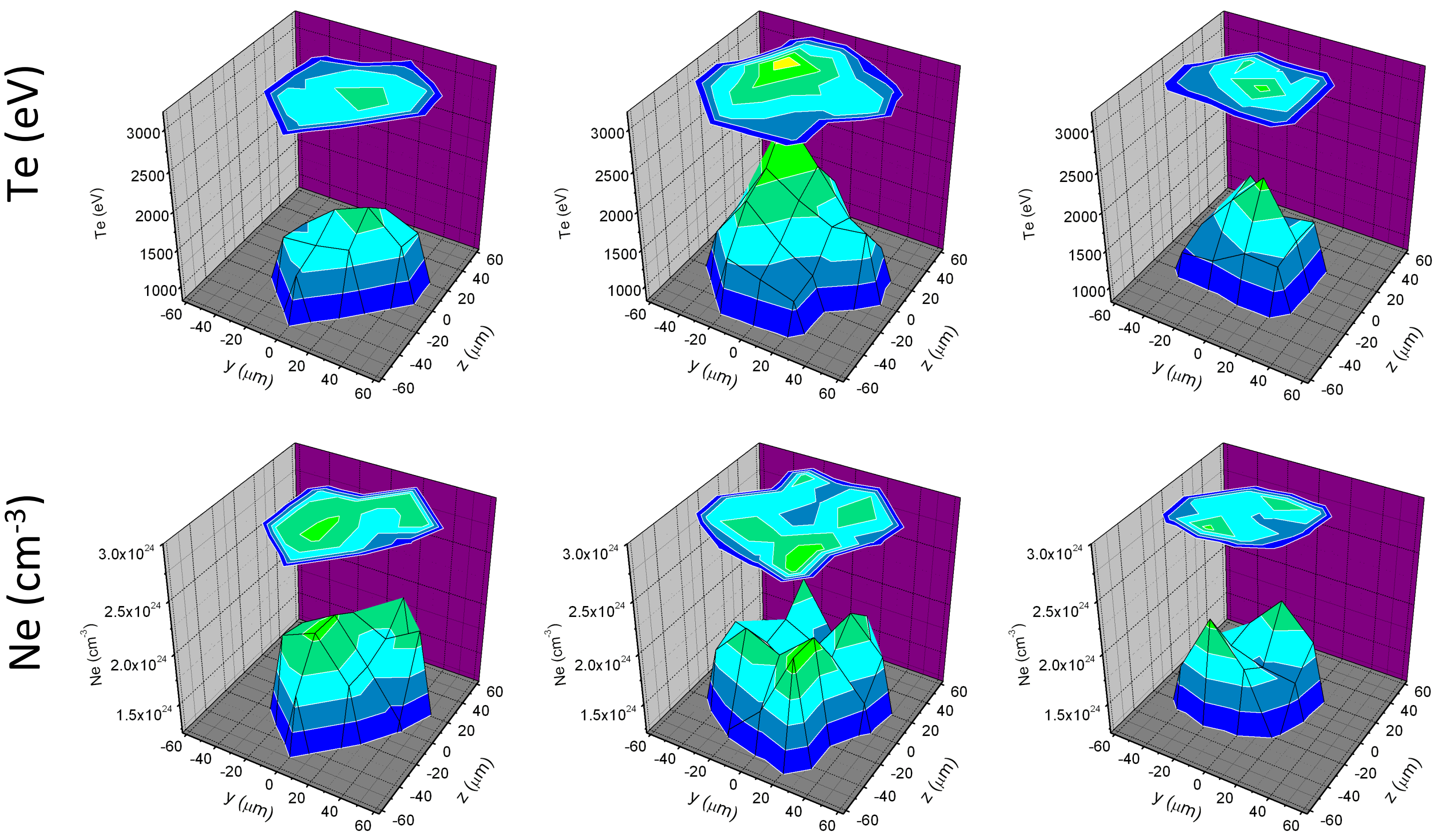

Constrain parameter[1]:
P_{const} = 2.9

[1]T. Nagayama, R. C. Mancini, R.Florido, D. Mayes, R. Tommasini, J. Koch, J. Delettrez, S. P. Regan, V. Smalyuk, Phys. Plasmas **19**, 082705 (2012)

The impact of atomic physics

- Atomic processes and plasma atomic kinetics determine,
  - ion charge state distribution and level populations
  - photon energy dependent emissivity and opacity
  - emission, absorption and transport of radiation
  - also to some extent, EOS and thermal transport

- Plasma perturbations result in Stark broadened line shapes

- As a consequence, atomic physics plays a key role in **both** the diagnosis and modeling of plasmas

- We illustrate and discuss these ideas with two examples,
  - plasma diagnosis: tracer x-ray spectroscopy of inertial confinement fusion implosions
  - plasma modeling: heating of photoionized plasmas driven by a broadband x-ray flux

Photoionized plasmas

- Widespread in space, e.g. active galactic nuclei warm absorbers, x-ray binaries, accreting disk surrounding black holes
- Plasma ionization is driven by an intense, broadband distribution of photons
- Unlike plasmas driven by a distribution of particles, photoionization and photoexcitation dominate atomic kinetics and drive plasma formation
- The complexity of the astrophysical environment makes the spectral analysis challenging ⟶ laboratory experiments are important[1]

Goals

- Perform systematic well characterized photoionized plasma experiments in the laboratory relevant to astrophysics
- Focus on plasma heating, ionization, and radiative properties
- **Guided by experimental observation, we seek to test and establish what physics models are needed to describe the plasma**

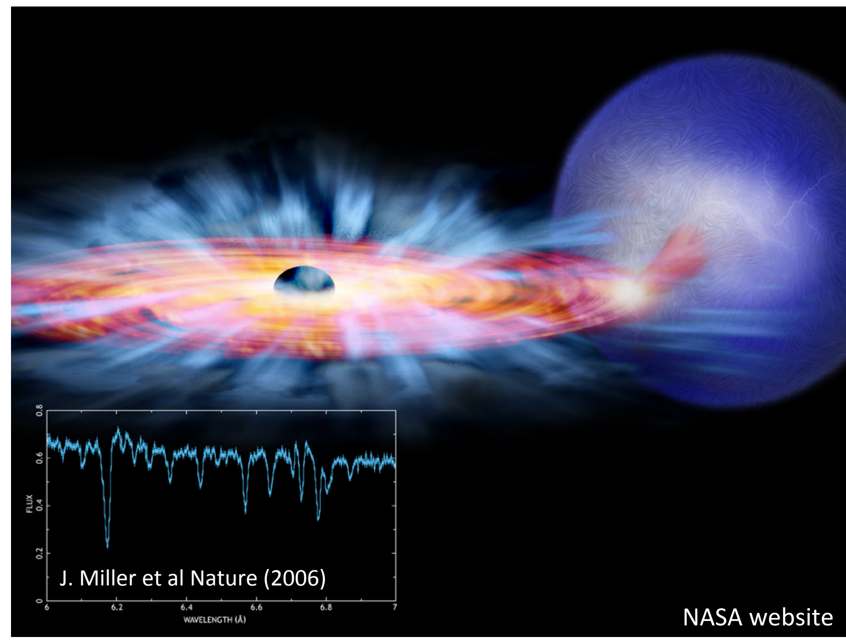

Artists impression of binary system GRO J1655-40, 11,000 lights years away in constellation Scorpius

[1]R. C. Mancini, J. E. Bailey, J. F. Hawley, T. Kallman et al, Phys. Plasmas **16**, 041001 (2009)

Experimental set up at Z

Experiments performed for filling pressures of neon in the range: 3.5 - 30 Torrs[1]

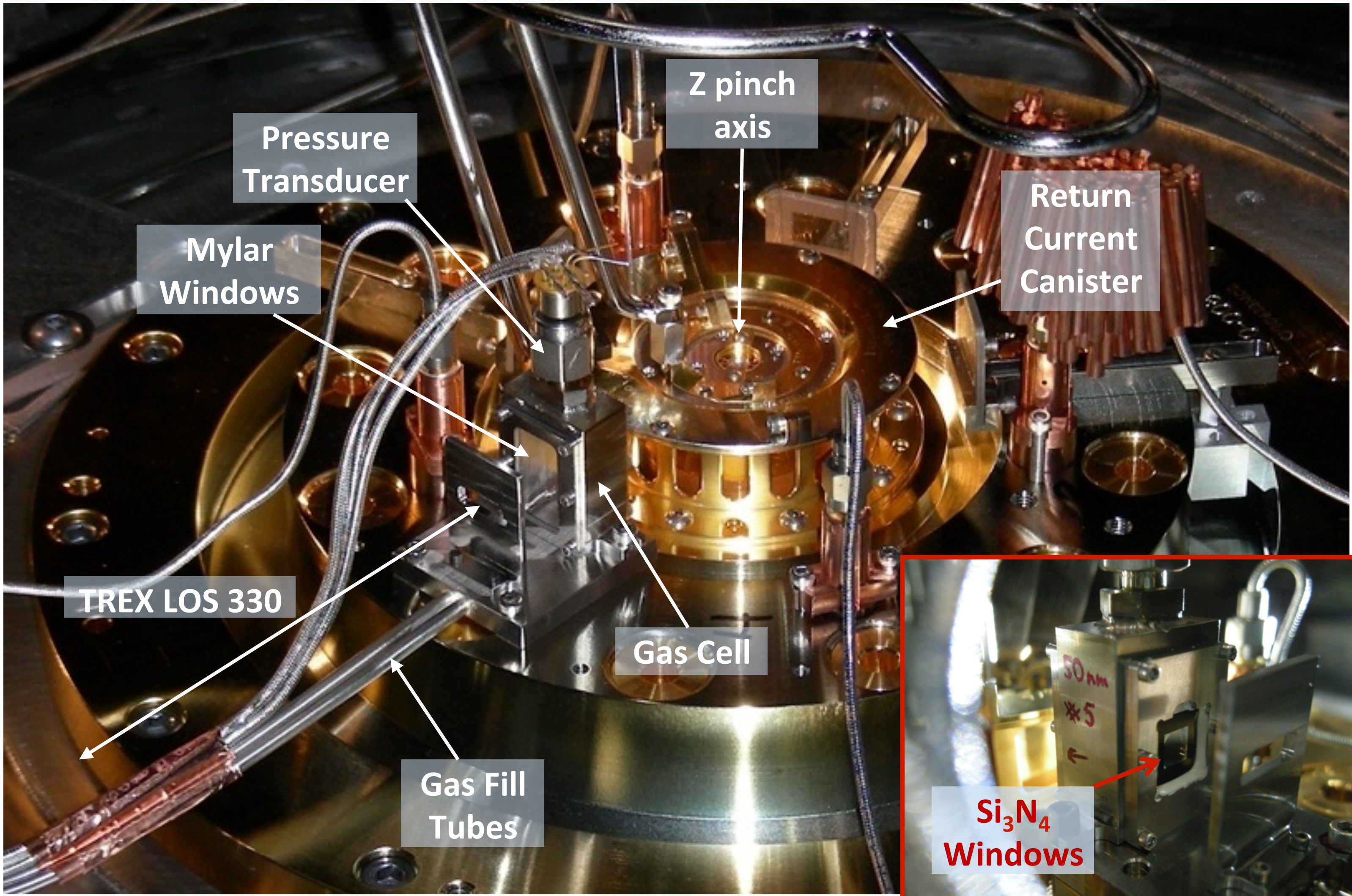

[1]I. M. Hall, T. Durmaz, R. C. Mancini, J. E. Bailey, G. A. Rochau et al, Phys. Plasmas **21** ,031203 (2014)
[2]**ZAPP** collaboration: G. A. Rochau, J. E. Bailey, R. E. Falcon, G. P. Loisel et al, Phys. Plasmas **21**, 056308 (2014)

Transmission spectrum displays K-shell line absorptions

Lines in Be-, Li-, He- and H-like ions show a highly ionized neon plasma

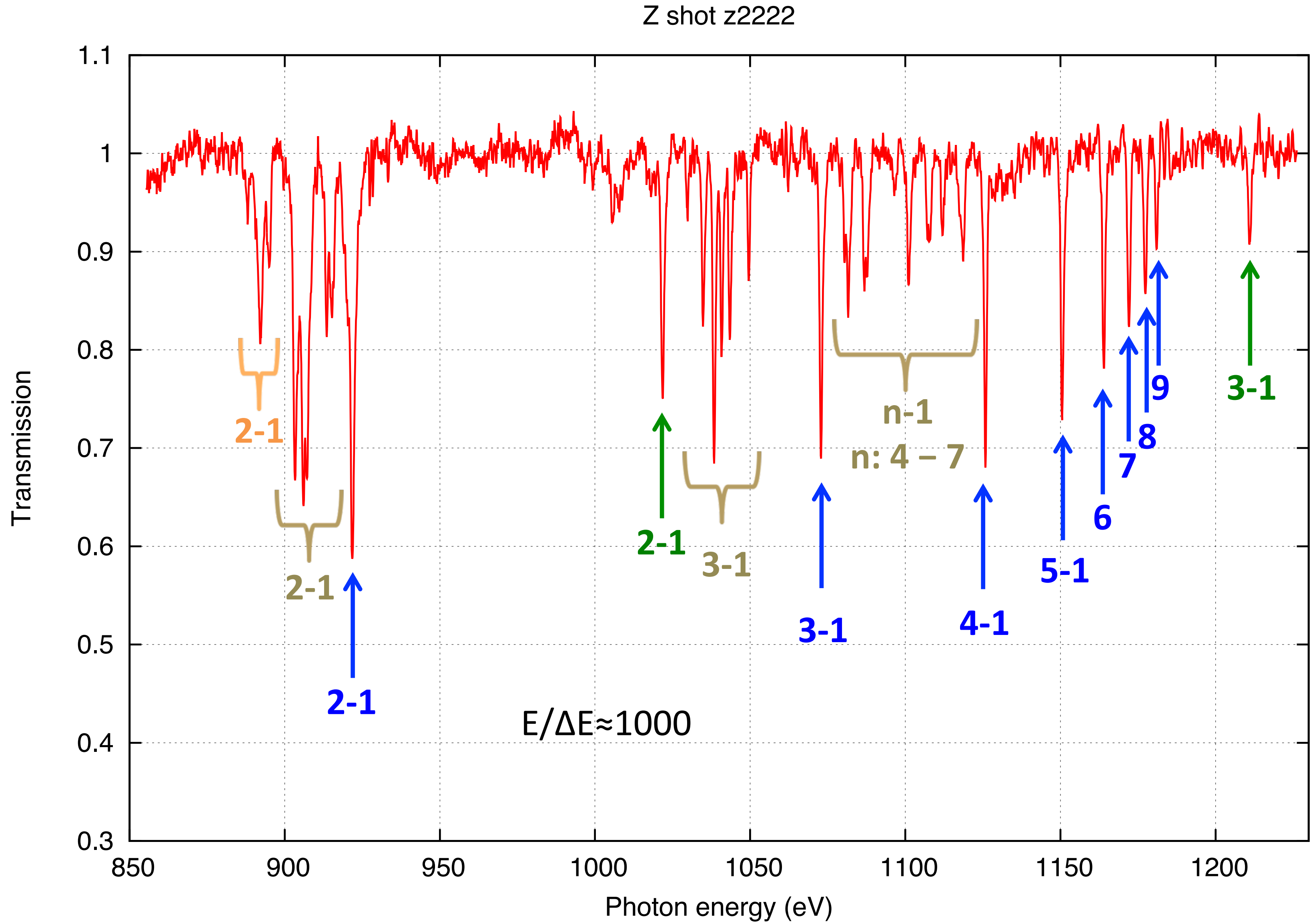

Extraction of charge state distribution

- Is it possible to extract the charge state distribution from data analysis without doing atomic kinetics calculations?
- Assume most of the population is in ground and low-excited states of ionization stages of Neon: $1s^22s^2$, $1s^22s2p$, $1s^22p^2$, $1s^22s$, $1s^22p$, $1s^2$, 1s
- Transmission $T_\nu = e^{-\tau_\nu}$, optical depth $\tau_\nu = k_\nu L$
- Opacity has many contributions $k_\nu = \sum_{l,u} \sigma_\nu^{l,u} N_l$, $\sigma_\nu = \frac{\pi e^2}{m_e c} f_{l.u} \phi_\nu$
- Substituting $T_\nu = e^{-\sum_{l,u} \sigma_\nu^{l,u} N_l L}$
- **Idea:** search for areal-densities $N_l L$ that yield the best fit to the experimental photon-energy dependent transmission
- How do we drive the search in parameter space? → Genetic Algorithm[1]

[1] I. E. Golovkin, R. C. Mancini, S. J. Louis et al, J. Quantitative Spectroscopy Radiative Transfer **75**, 625 (2000)

Electron temperature T_e estimation

- Li-like neon population ratio $1s^22p/1s^22s$ is dominated by collisions
- This population ratio can be determined from the analysis of the transmission spectrum, and used to extract **T_e= 19±4eV**
- Tested with atomic kinetics modeling, and synthetic data analysis
- Also applied in Si photoionized plasma experiment

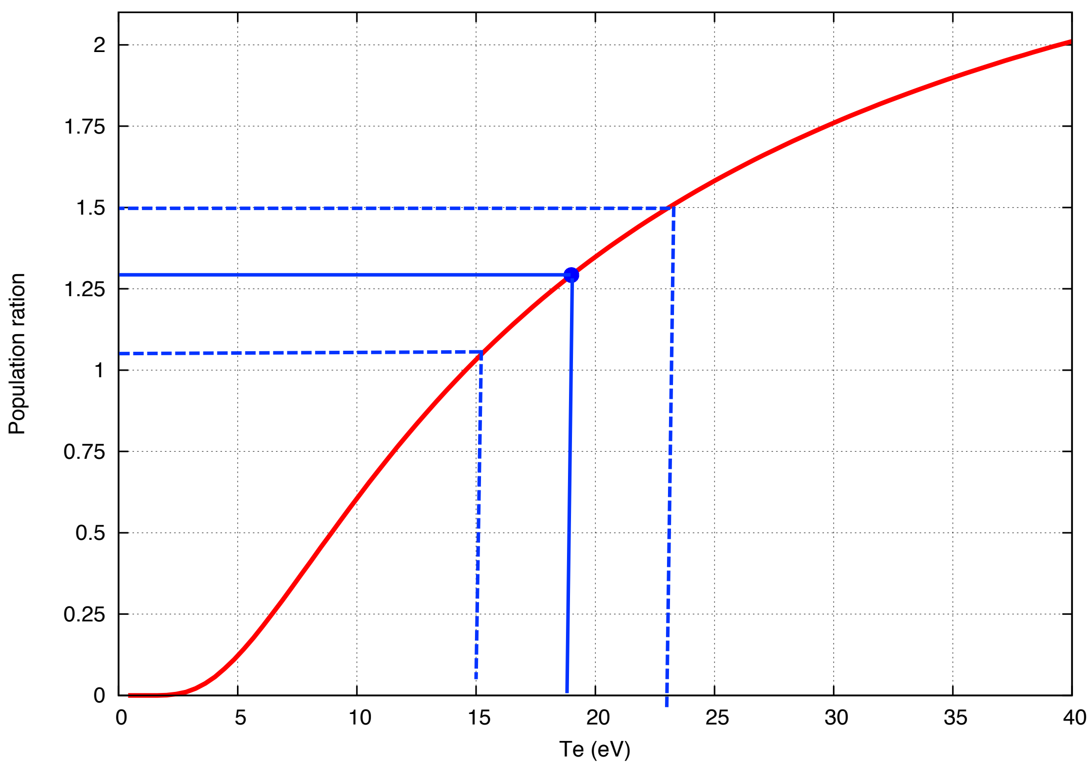

$$R = g e^{-\frac{\Delta E}{kT_e}}$$

$$g = 3$$

$$\Delta E = 16eV$$

$$\frac{\delta T_e}{T_e} = \left(\frac{kT_e}{\Delta E}\right)\frac{\delta R}{R}$$

Modeling strategy: three parts

- X-ray flux
  - 3D view-factor code VISRAD[1] to model x-ray flux impinging on photoionization sample, constrained by experimental measurements
- Boltzmann electron kinetics
  - Self-consistent and simultaneous electron and configuration-average atomic kinetics[2] to determine the electron distribution function and a first approximation of the ion charge-state distribution
- Radiation hydrodynamics
  - Assuming electrons are in equilibrium, HeliosCR[3] radiation-hydrodynamics simulations of the experiment to account for the effects of window transmission, hydrodynamics, non-equilibrium atomic physics, and photon-energy resolved radiation transport

[1]J. J. MacFarlane, J. Quantitative Spectroscopy Radiative Transfer **81**, 287 (2003)
[2]J. Abdallah, Jr. et al, J. Physics B **45**, 035701 (2012)
[3]J. J. MacFarlane, I. E. Golovkin and P. R. Woodruff, J. Quantitative Spectroscopy Radiative Transfer **99**, 381 (2006)

X-ray drive spectral distribution

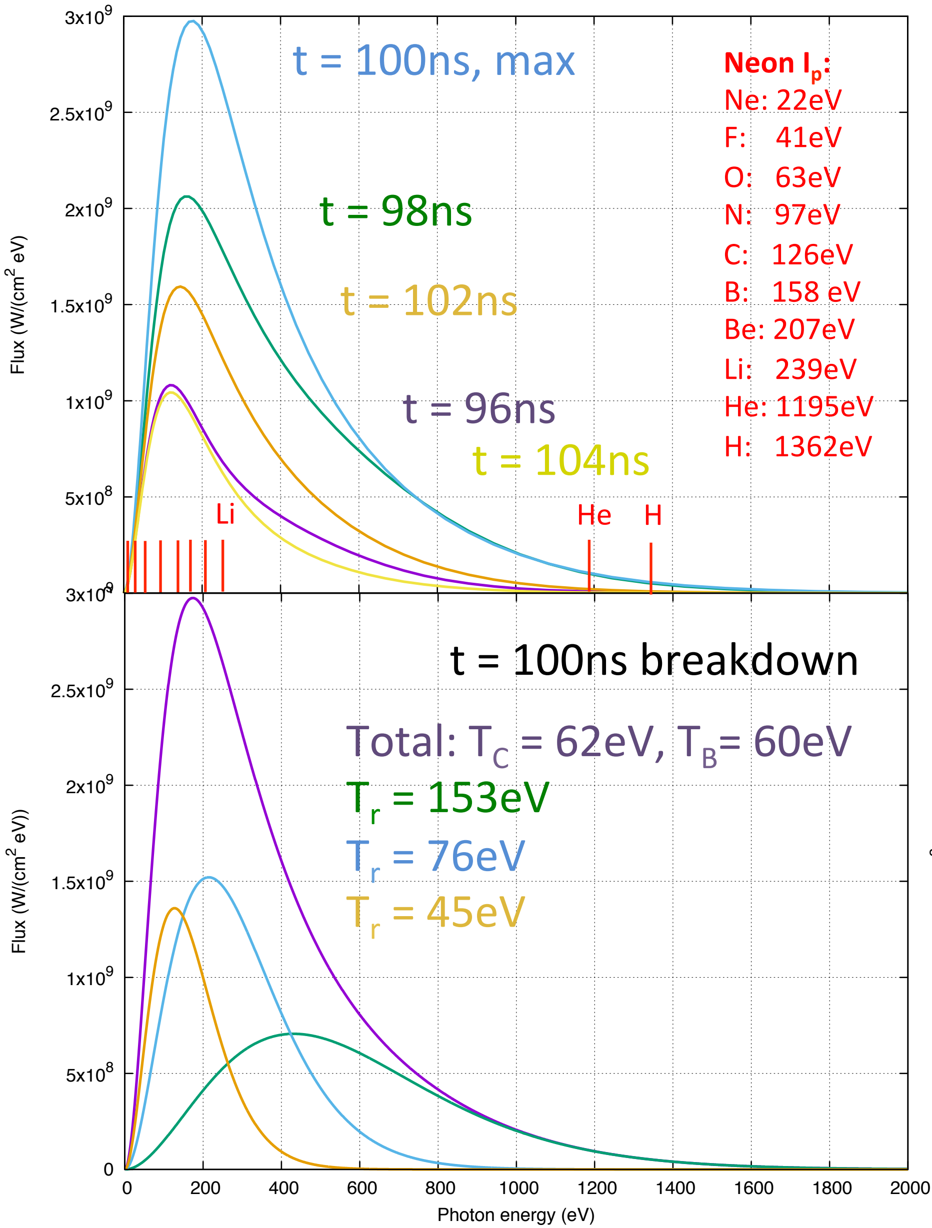

- Modeled with view factor code VISRAD constrained with x-ray power, pinch size, and source brightness distribution data
- Well approximated with three scaled Planckian distributions
- Transmission through Mylar window attenuates x-ray drive

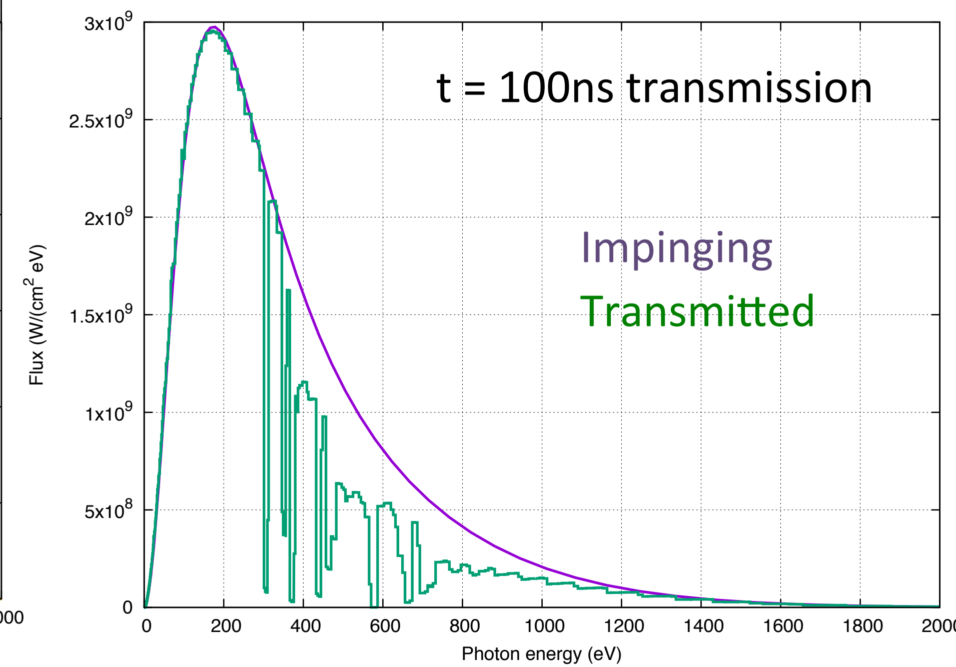

Boltzmann electron kinetics

- Self-consistent solution of time-dependent electron and atomic kinetics[1-4]
- Electron kinetics: Boltzmann equation for electron distribution function
- Assume uniform plasma, zero-D model, and no external forces

$$\frac{df}{dt} = \frac{\partial f}{\partial t} + \frac{\vec{p}}{m} \cdot \vec{\nabla}_r f + \frac{\vec{F}}{m} \cdot \vec{\nabla}_v f \approx \frac{\partial f}{\partial t} = K_{ee}(f) + K_{inel}(\vec{N}, f)$$

- K_{ee}: electron-electron elastic scattering
- K_{inel}: electron-ion atomic processes

- Atomic kinetics: set of collisional-radiative (CR) atomic rate equations

$$\frac{d\vec{N}}{dt} = A(f)\vec{N}$$

- Input: total atom number density from neon gas fill pressure,
  time-history of spectrally resolved x-ray flux $F_\nu(t)$

[1]J. Abdallah, Jr. et al, Phys. Rev. A **68**, 63201 (2003)
[2]M. E. Sherrill et al, J. Quant. Spectrosc. Rad. Transfer **99**, 584 (2006)
[3]M. E. Sherrill et al, Phys. Rev. E **73**, 066404 (2006)
[4]J. Abdallah, Jr. et al, J. Physics B **45**, 035701 (2012)

Atomic model for Boltzmann electron kinetics

- Atomic processes included:
  - electron collisional excitation and deexcitation
  - spontaneous radiative decay
  - electron collisional ionization and (3B) recombination
  - resonant electron capture and autoionization
  - electron radiative recombination
  - free-free (Bremsstrahlung) emission
  - free-free (inverse Bremsstrahlung) driven by x-ray drive
  - photoexcitation and photoionization driven by x-ray drive
- Optically thin approximation: no trapping of line transition, radiative recombination and Bremsstrahlung self-emission photons
- Neon atomic model:
  - configuration average approximation
  - non-autoionizing and autoionizing states included
  - 2054 configurations, all ionization stages

Atomic processes impact the electron distribution (I)

- Electron-ion collisions contribute to the heating and cooling of **free electrons**

Heating	Cooling
electron collisional deexcitation	electron collisional excitation
electron collisional (3B) recombination	electron collisional ionization
free-free (inverse Bremsstrahlung) absorption driven by x-ray flux	free-free (Bremsstrahlung) emission

- **Free electrons** are added and removed by atomic ionization and recombination

Ionization	Recombination
electron collisional ionization	electron collisional (3B) recombination
Photoionization driven by x-ray flux (adds energy to pool of free electrons)	electron radiative recombination
No photoionization driven by plasma self-emission: model is "optically thin"	
spontaneous autoionization (also adds energy to pool of **free electrons**)	resonant electron capture

Atomic processes impact the electron distribution (II)

- Photon excitation and deexcitation of atomic levels indirectly affect the distribution of **free electrons**

Atomic excitation	Atomic deexcitation
Photoexcitation driven by x-ray flux	spontaneous radiative decay
No photoexcitation driven by plasma self-emission: model is optically thin	

- The distribution of **free electrons** is thermalized by electron-electron elastic scattering

- Electron-ion scattering is not included

Electron energy distribution function

Free electrons thermalize quickly and evolve through a series of equilibrium states

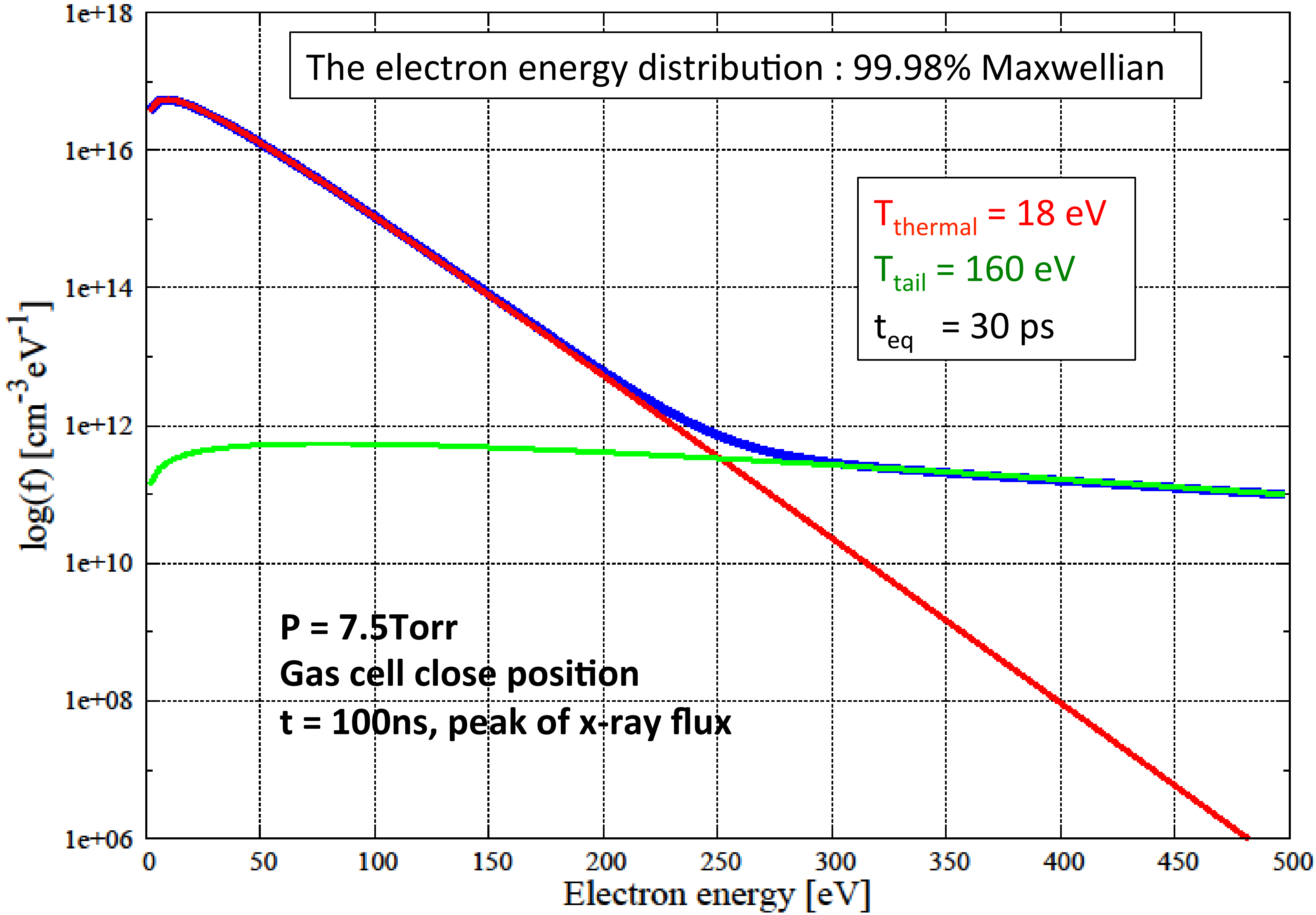

Radiation-hydrodynamics simulations

- Helios-CR radiation-hydrodynamics model and code[1]
- Complete system: front window + neon + rear window
- Standard 1-D Lagrangian hydrodynamics
- Advanced atomic physics and radiation transport
- Photon-energy resolved emissivity and opacity computed with inline atomic kinetics
- For the same atomic model, two approximations:
  - Level population distribution from LTE solution of atomic kinetics: **equilibrium atomic physics**
  - Level population distribution from solution of time-dep. CR atomic kinetics: **non-equilibrium atomic physics**
- **Non-equilibrium atomic physics directly couples the x-ray flux to the atomic kinetics**
- Multi-angle, photon-energy resolved radiation transport
- Equilibrium equation of state

[1]J. J. MacFarlane, I. E. Golovkin and P. R. Woodruff, J. Quant. Spectrosc. Rad. Transfer **99**, 381 (2006)

X-ray flux heats neon photoionized plasma uniformly

- But, the radiation heating and cooling rates modeled with inline NLTE or LTE atomic kinetics are different, P=30Torr, t=100ns

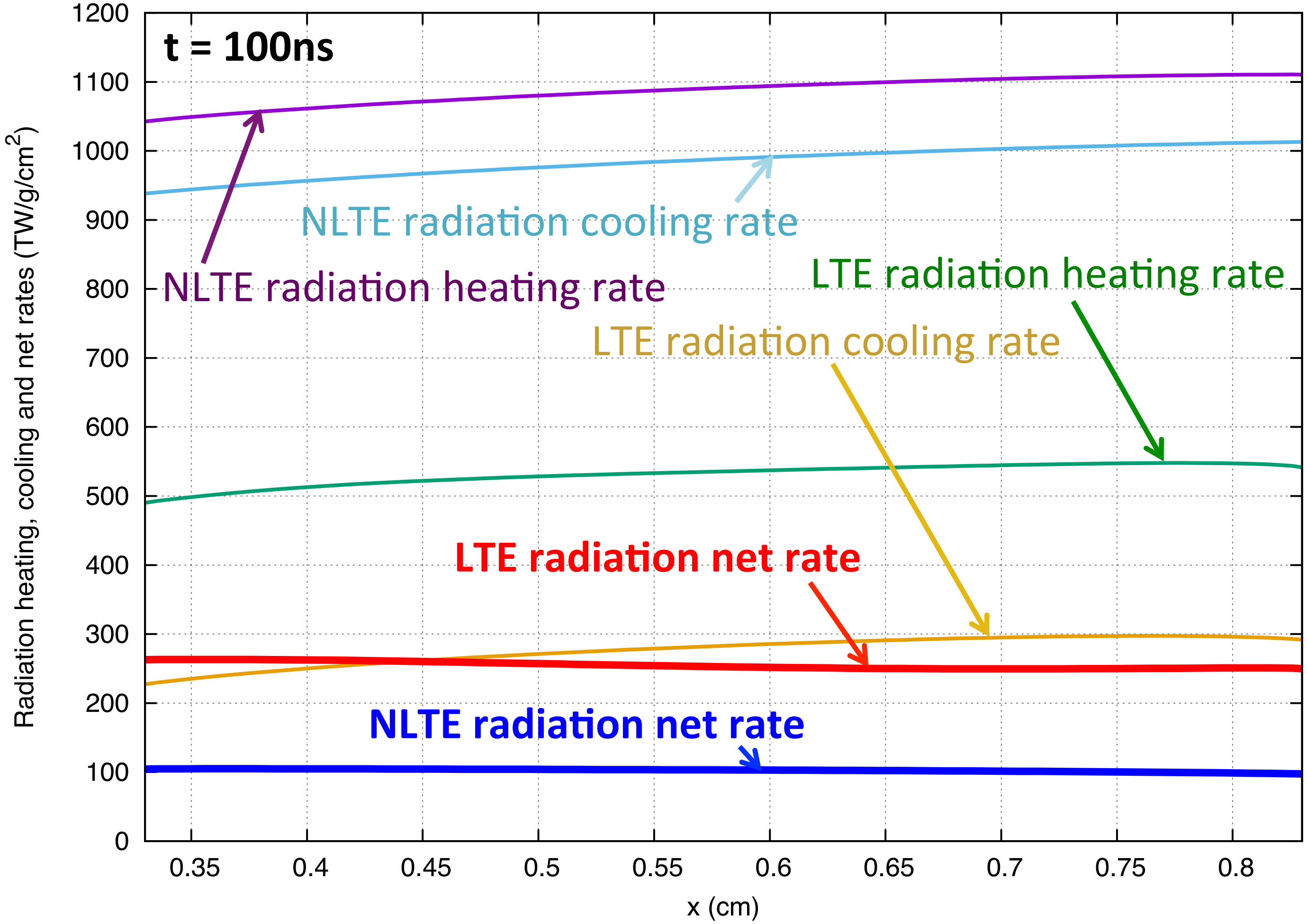

X-ray heating depends on drive and plasma conditions

Radiation rates peak before x-ray drive

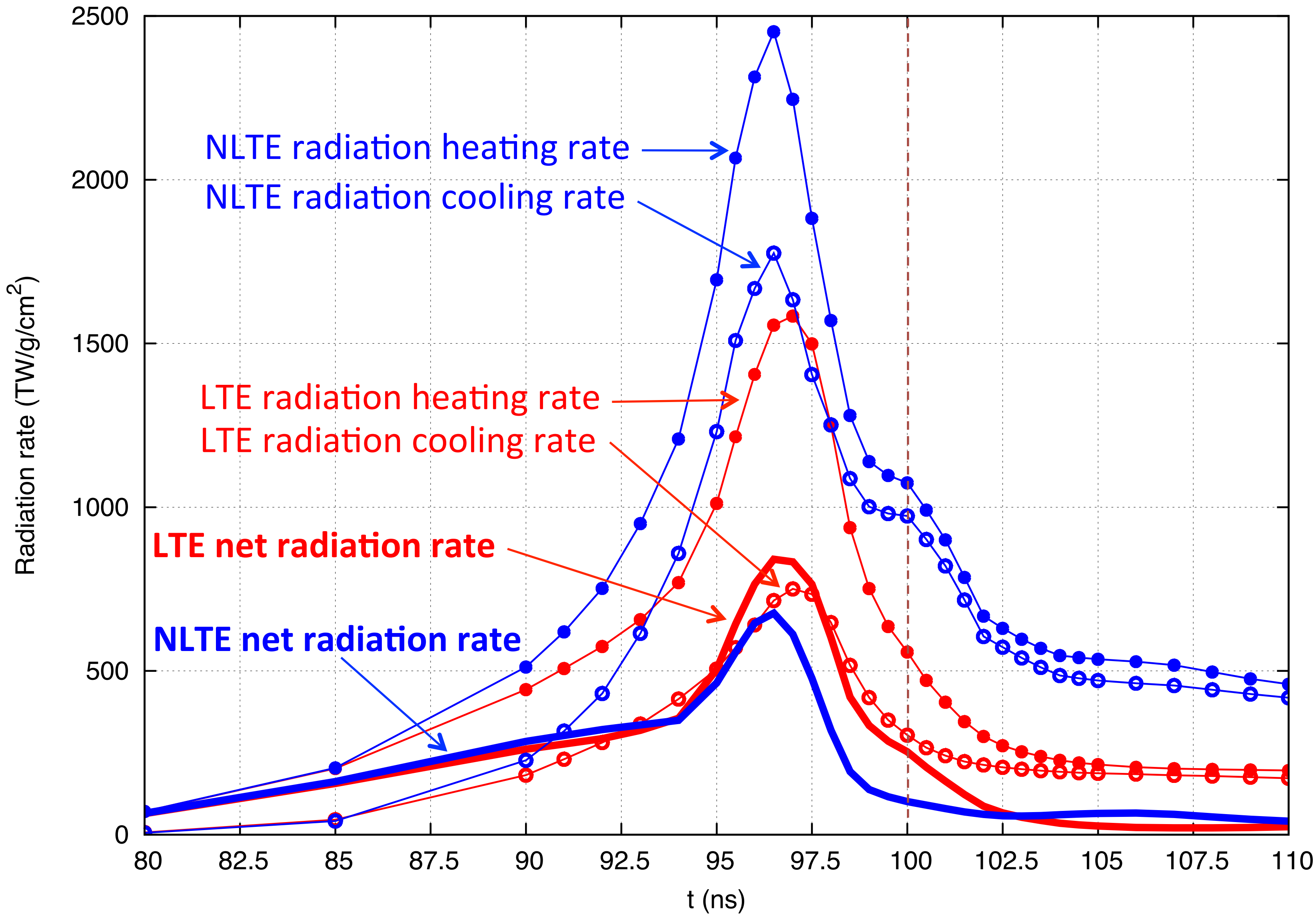

Atomic physics modeling impacts x-ray heating

Non-equilibrium x-ray heating produces lower T_e more consistent with observation

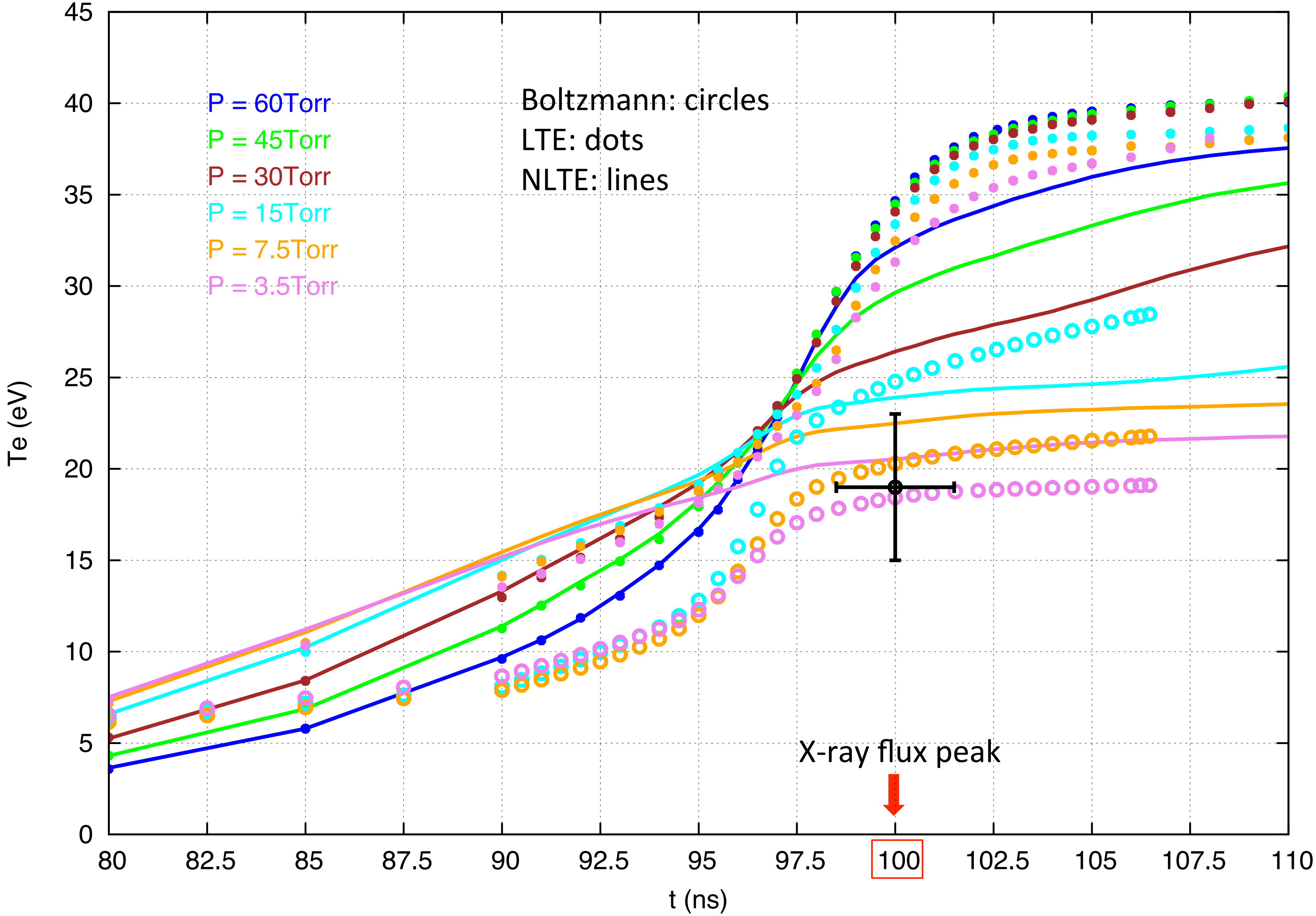

Astrophysics models overestimate T_e

- Astrophysics modeling codes Cloudy[1] and XSTAR[2] were used to calculate plasma heating and electron temperature T_e
- Self-consistent solution of collisional-radiative atomic kinetics, energy balance, and radiation transport
- These models are steady state, consider P=30Torr and P=60Torr

P (Torr)	Cloudy T_e (eV)	XSTAR T_e (eV)
30	55	65
60	45	57

- Both models overestimate the electron temperature, Cloudy less than XSTAR

[1]G. Ferland et al, Publ. Astron. Soc. Pacific **110**, 761 (1998)
[2]T. Kallman and M. Bautista, Astrophys. J. Sup. Series **133**, 221 (2001)

Conclusions

- Atomic physics impacts **both** plasma diagnosis and modeling
- Two cases were discussed,
  - tracer x-ray spectroscopy of ICF implosion experiments
  - x-ray heating of laboratory photoionized plasmas
- NLTE atomic kinetics, **spectral line shapes**, and radiation transport are key for modeling the emergent intensity distribution
- There is a need to improve current electron broadening models, and ion broadening of L-shell spectra
- **Multi-objective data analysis** in HEDP is relatively new, it has been very useful and it is changing the way we use data, how can we connect the PGA to other methods/ideas such as MCMC?
- We are just beginning to see the interplay between **atomic kinetics and heating of photoionized plasmas**, laboratory experiments have been and will continue to be critical

This work was sponsored in part by DOE/NLUF Grants DE-NA0000859 and DE-NA0002267, DOE NNSA Grant DE-FG52-09NA29551, DOE OFES Grant DE-SC0014451, LLNL, and the Z Facility Fundamental Science Program of SNL